THESIS

PLASMA BREAKDOWN IN SULFUR HEXAFLUORIDE AND AIR MIXTURES FOR HIGH VOLTAGE SWITCH APPLICATIONS

Submitted by

Evan J. Ronzone

Department of Mechanical Engineering

In partial fulfillment of the requirements

For the Degree of Master of Science

Colorado State University

Fort Collins, Colorado

Summer 2025

Master's Committee:

Advisor: Azer P. Yalin

John D. Williams
Steven J. Simske

ABSTRACT

PLASMA BREAKDOWN IN SULFUR HEXAFLUORIDE AND AIR MIXTURES IN HIGH VOLTAGE SWITCHES

High voltage spark gap switches are critical components used across a wide range of electrical systems where reliable switching and protection at high voltage is required. Power transmission and generation systems rely on such switches to protect systems in the event of switching surges, while also functioning as switching elements in high-voltage circuit breakers. High voltage spark gaps enable the controlled delivery of enormous amounts of electrical energy in very fast timescales. Such properties make spark gap switches highly desirable for pulsed power facilities such as Sandia National Laboratories Z-Machine. Across all applications, these switches must reliably hold off very high voltages on the order of hundreds of kilovolts, while maintaining accurate function. Switchgear must operate for long periods of time, with minimal maintenance. Spark gaps commonly use dielectric gas to insulate the electrodes and improve performance. Among such gases, sulfur hexafluoride (SF_6) has been the preferred choice due to its excellent breakdown and recombination qualities.

Sulfur hexafluoride possesses exceptional dielectric strength due to its large molecular size and high electronegativity, which allows it to effectively capture free electrons and prevent avalanche breakdown in high electric fields. Additionally, SF_6 demonstrates superior recombination properties, as its dissociation products tend to recombine back into stable SF_6 molecules, maintaining consistent gas composition and breakdown voltage over many switch

closures. However, SF_6 is also an expensive gas which presents significant supply chain challenges. SF_6 also presents a major asphyxiation hazard in the event of a leak. Efforts to remove SF_6 from current high voltage systems require significant design revisions and are difficult to implement quickly. A possible solution to reduce SF_6 usage is to use a mixture of SF_6 and zero-air (synthetic air nominally composed of 79% N_2 and 21% O_2, with trace impurities typically below 1 ppm total) at higher operating pressure. However, such mixtures do not yet have large amounts of data supporting their breakdown properties or long-term reliability.

This thesis presents the design of an experimental system that measures the breakdown voltages of zero-air - SF_6 mixtures at varying operating pressures and compositions. Long-term measurements of breakdown voltage stability and switch reliability using Weibull analysis are also presented. The theoretical background of Paschen's law is discussed, including linear approximations in high pressure-distance ranges. Significant efforts were undertaken to accurately measure the voltage immediately prior to breakdown by minimizing free variables and losses. New switch designs were created, and significant system alterations were made to improve data collection accuracy. System automation was enhanced to accommodate very long test series which would otherwise require significant manual labor over many days.

Results indicate that relatively small concentrations of SF_6 in gas mixtures significantly increase breakdown voltage compared to pure air. Furthermore, repeated breakdown testing of these mixtures demonstrates comparable, though slightly reduced, reliability compared to pure SF_6. Future investigations examining breakdown products or electrode surface conditions could provide better understanding of the recombination dynamics in these mixed-gas systems.

TABLE OF CONTENTS

LIST OF FIGURES

SAND2025-08262T

Sandia National Laboratories is a multimission laboratory managed and operated by National Technology & Engineering Solutions of Sandia, LLC, a wholly owned subsidiary of Honeywell International Inc., for the U.S. Department of Energy's National Nuclear Security Administration under contract DE-NA0003525.

This paper describes objective technical results and analysis. Any subjective views or opinions that might be expressed in the paper do not necessarily represent the views of the U.S. Department of Energy or the United States Government.

1. **Introduction and Background**

1.1 High Voltage Switches and Pulsed Power

The Pulsed Power and Plasma Science Center (P3SC) at Colorado State University (CSU) was developed with assistance from Sandia National Laboratories (SNL) to analyze high voltage switchgear in use on their pulsed power systems [1]. Pulsed power is the process of using a low-power source to slowly charge and store large amounts of electrical energy. This energy is then rapidly discharged in a single, compressed pulse [2]. This resulting pulse occurs over very small timescales, creating immense power concentrations. Pulsed power was swiftly adopted by the fusion community, primarily for the continued study of Inertial Confinement Fusion (ICF). One method to achieve ICF conditions is to deliver a very large amount of power to a very small target, forcing it to ionize into a plasma that implodes due to intense magnetic fields created by the pulse of current. The compressed plasma can then reach high temperatures suitable for fusion conditions [3], [4].

One such example of a pulsed power machine is SNL's Z-Machine (Figure 1), which utilizes pulsed power to create the world's most powerful radiation source [3]. The Z-machine operates by storing electrical energy in 36 separate megavolt-class Marx banks. Each Marx bank consists of sixty capacitors, that are slowly charged in parallel to the desired voltage. When ready to fire, these Marx banks are discharged in series, adding the stored voltages to create a megavolt class pulse [5]. This pulse is then sent to an intermediate store capacitor, which briefly stores the energy before a High Voltage Laser Triggered Switch (HV-LTS) which is then used to individually switch over this stored energy, sending it to the pulse forming coaxial lines. These lines then lead

to a self-breaking water switch that sharpens the pulse, before the voltage is finally sent to magnetically insulated transmission lines and then to the load [1], [6].

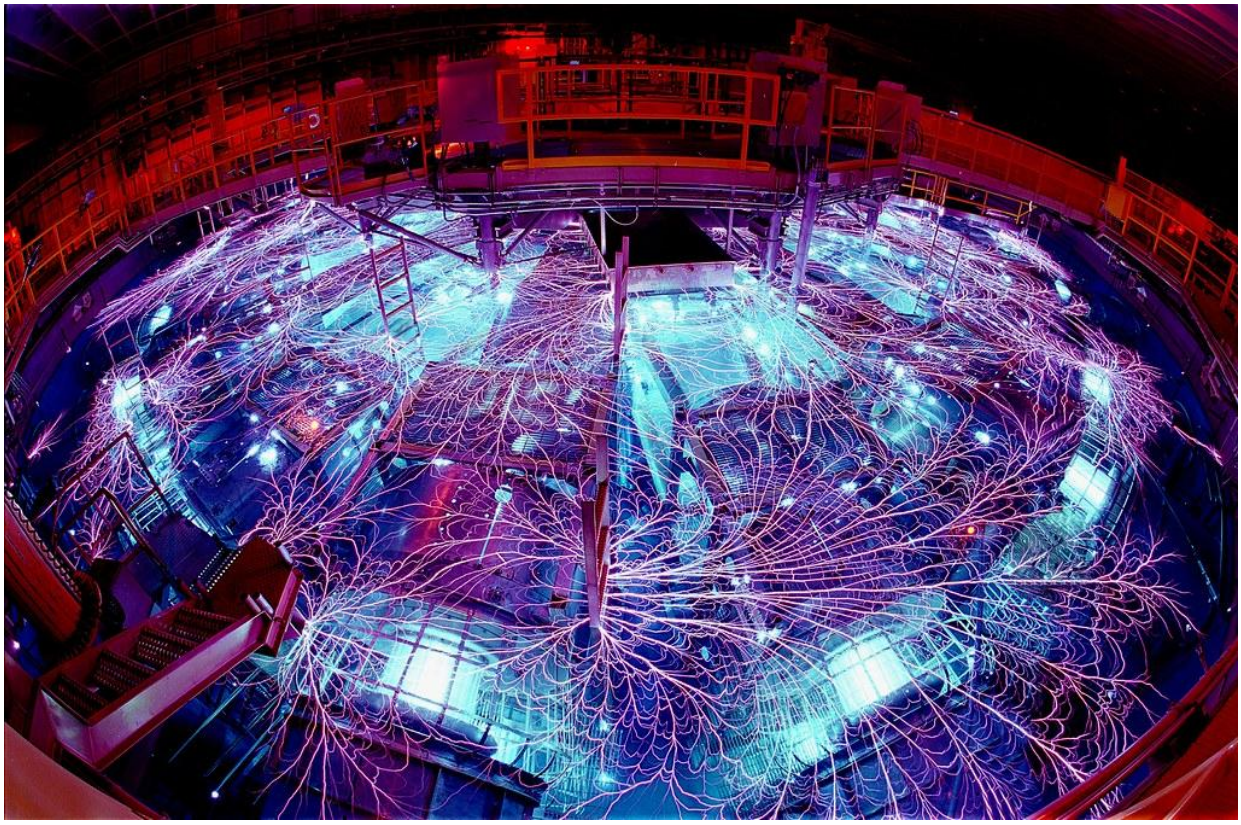

Figure 1: Z-Machine. Credit: https://www.sandia.gov/z-machine/.

Each store capacitor has its own HV-LTS, this allows for staggering of the trigger time and allows researchers to tailor the output characteristics of the machine. These switches must be carefully timed and controlled due to the immense voltages involved [7], [8]. Such switches are typically insulated using SF_6 at reasonably high pressure. The P3SC was originally designed to further examine HV-LTS behavior in cooperation with SNL [1]. A system that replicated similar conditions to the store capacitor and HV-LTS (Figure 2) was studied using optical and electrical diagnostics such as Thomson scattering [9]. The objective of this work was to examine the

behavior of controlled breakdowns by laser triggering and the validity of the Martin-Braginskii Switch model in new, low-impedance switches [10].

Now, the P3SC's focus has shifted to research alternative gas mixtures to help reduce SF_6 usage in switchgear at the national lab. To utilize these gas mixtures effectively in HV-LTS's the self-break voltage for a given gas at a specified pressure must be known.

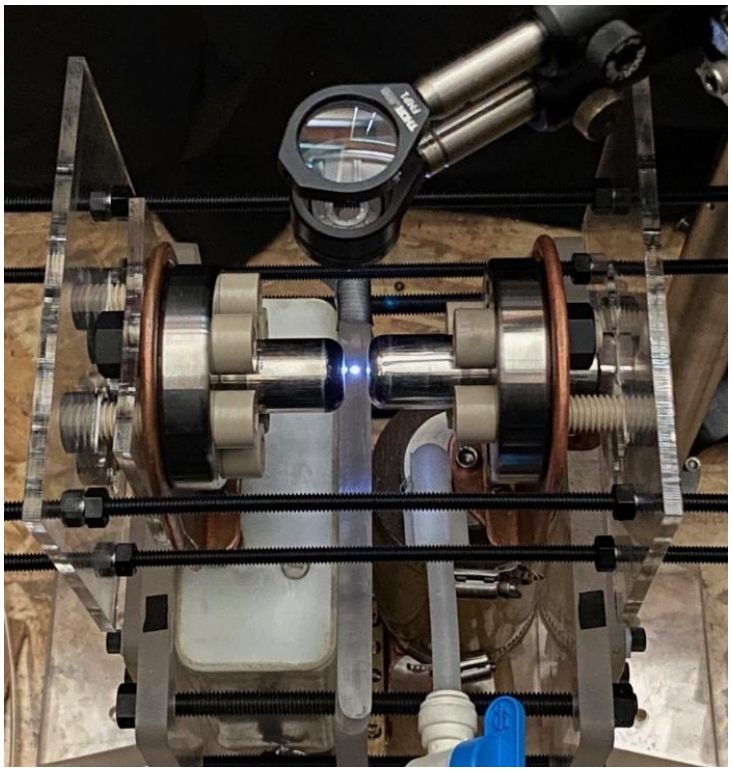

Figure 2: HV-LTS open setup at CSU P3SC.

Many high voltage switch designs use spark gaps [11]. Spark gaps operate by using a gas at a given pressure spaced apart from each other by a distance. The set of electrodes are charged to a high voltage, with one electrode leading to the load, and then to ground. This high potential across the gap creates an electric field. If the field is of sufficient strength, the gas then rapidly ionizes via electron avalanche ionization, creating a conductive plasma [11], [12]. This plasma then connects the two electrodes by streamer propagation, allowing current to flow effectively

closing the switch [13], [14]. This process is spontaneous, and timing can be challenging to control when the electrodes are brought to sufficient breakdown voltage. Thus, many switches in use are not brought to their breakdown voltage, but rather a percentage of this voltage. Then, a triggering mechanism such as a laser pulse can be used to initiate breakdown [1], [10], [15], [16]. This percentage of self-break requires known self-breakdown voltages, which are specific for every gas or gas mixture. To calculate these voltages, Paschen's Law is commonly used.

1.2 Townsend Discharge and Paschen's Law

Paschen's Law describes the breakdown voltage (V_B) required for a particular gas to ionize and form an arc between two electrodes as a function of the product of the pressure and gap distance (i.e., pd) [17]. This law is derived from Townsend discharge, also called electron avalanche ionization, occurring in the gas [18], [19]. Paschen's Law, which governs the breakdown voltage, V_B, is expressed as:

$$V_B = \frac{Bpd}{\ln(Apd) - \ln\left(\ln(1 + 1/\gamma)\right)} \tag{1}$$

where A and B are gas – dependent constants from Townsend's first ionization coefficient, γ is the secondary electron emission coefficient from the cathode, p is the pressure, and d is the gap spacing. To get coefficients A and B, one must first examine the Townsend Breakdown criterion for a self-sustained discharge in a gas [20]. The first Townsend coefficient α represents the number of ionizing collisions made by a single electron per unit length [21]. α can be modeled with the following equation for a uniform electric field condition:

$$\alpha = Ap * e^{-\frac{Bp}{E}} \tag{2}$$

where E is the average electric field in the gap, A is the ionization frequency scaling factor, and B is the ionization energy threshold parameter.

A is a constant which quantifies the number of ionizing collisions per unit length per unit pressure in a sufficiently strong electric field. It represents how easily electrons in a particular gas can initiate ionization. B is a constant which quantifies the required energy for an electron to gain before it can ionize a neutral gas molecule. Both of these constants are dependent on the gas used as the breakdown medium [22]. By using standardly accepted values of A, B, and γ for air and SF_6 from literature [23], theoretical Paschen curves were generated in Figure 3.

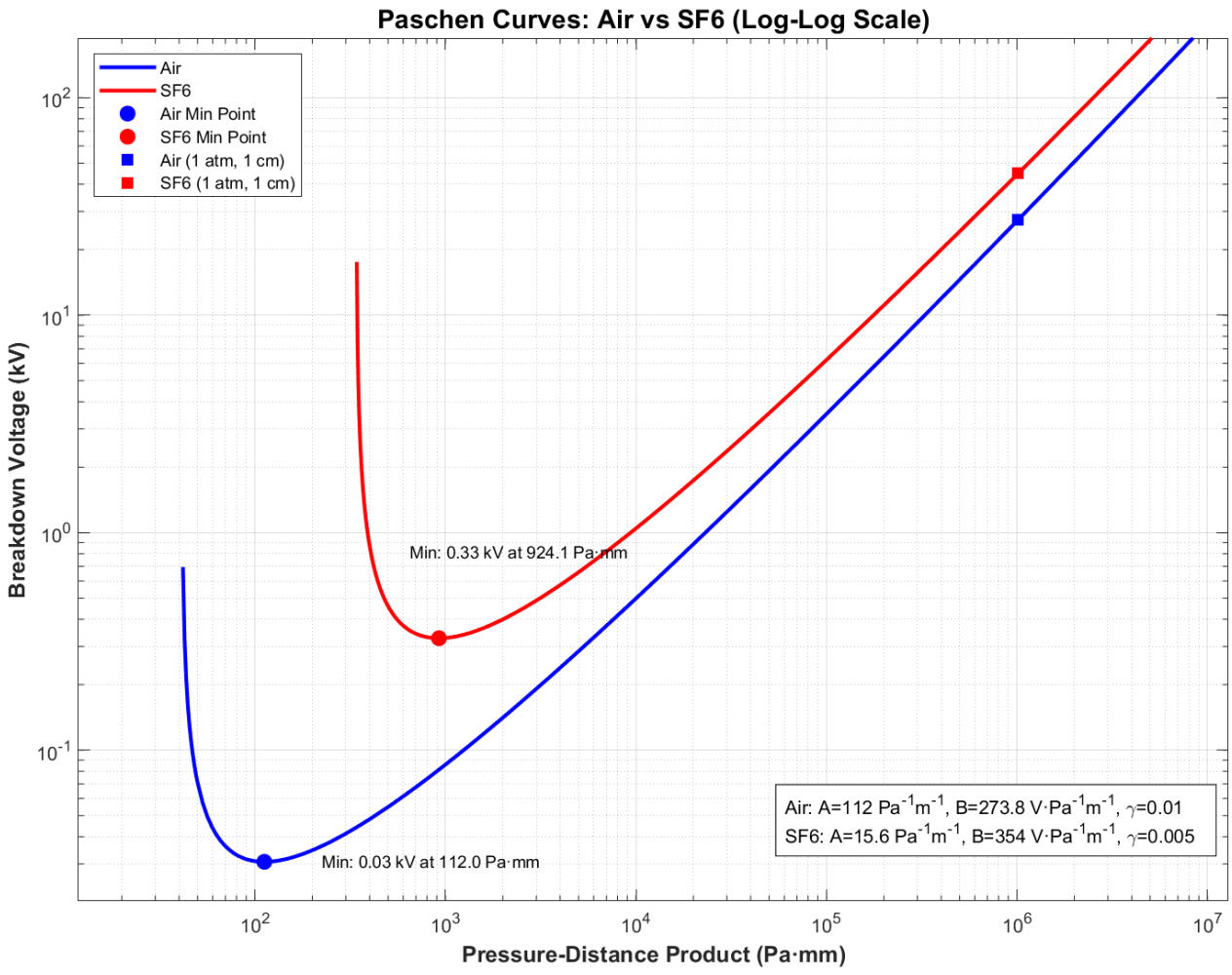

Figure 3: Theoretical Paschen curves with standard A, B, and γ values.

1.3 The Martin – Braginskii Switch Model

Many systems which use high voltage spark gaps require precise timing and low jitter. The model currently used to predict the behavior of plasma in high voltage switches is the Martin - Braginskii model [24], [25]. This model was originally created by Braginskii during his studies on lightning formation in 1958. After breakdown occurs at the voltage predicted by equation (1) and the plasma channel connects the anode and cathode, current begins to flow through the completed channel of plasma. Joule heating is the dominant energy addition mechanism. This heating causes the channel to widen, and the energy is dissipated once the driving current ceases.

Braginskii treats the outermost plasma front as a "piston" traveling at supersonic speeds. This piston drives a shock front which ionizes the background gas. Braginskii then uses several assumptions to solve the conservation equations of continuity, motion, and energy. These assumptions include cylindrical symmetry, fully ionized collisional plasma, Spitzer resistivity, no losses except from expansion, and electron-ion collisions. Braginskii starts with the electron energy equation in cylindrical coordinates [26]:

$$\frac{d}{dt}\left(\frac{3}{2}n_e k_B T_e\right) = \sigma j^2 + \nabla \cdot (\kappa_e \nabla T_e) \tag{3}$$

where n_e is the electron density, T_e is the electron temperature, σ is Spitzer electrical resistivity, j is current density, and κ_e is Spitzer thermal conductivity. For a resistive heating mechanism, Spitzer resistivity is used to compute the electrical resistivity:

$$\sigma j^2 = \sigma_0 T_e^{-\frac{3}{2}} \left(\frac{I(t)}{\pi r(t)^2}\right)^2 \tag{4}$$

Then, this resistivity is used to compute the thermal conductivity, assuming radial heat transport due to the cylindrical nature of the plasma:

$$\nabla \cdot (\kappa_e \nabla T_e) \approx -\frac{\kappa_e T_e}{r^2} \tag{5}$$

Braginskii then assumes constant density and then estimates thermal pressure to drive the expansion of the plasma channel. He then uses experimental data to determine a final relationship between plasma radius and current:

$$r(t) \propto \left(\frac{\eta_0 I_0^2}{\rho}\right)^{\frac{1}{4}} \tag{6}$$

Where ρ is the density. He then arrives at the expression of radial expansion:

$$r(t) = At^k \tag{7}$$

Where A and k are constants associated the channel growth. Tom Martin then adapted this model to determine plasma resistivity and expresses radial growth as:

$$\frac{I^2}{\sigma} = 2\pi^2 \rho_0 \zeta (\dot{r} r)^3 \tag{8}$$

Where r is the plasma channel radius and $\dot{r}$ is the first time derivative. ζ is defined as:

$$\zeta = \kappa_e \left(1 + \frac{2 - k^{-1}}{\gamma - 1}\right) \tag{9}$$

Where γ is the ratio of specific heats, and k is the same constant in equation (7). Given this, equation (8) can be rewritten and integrated:

$$\left(\frac{4}{\sigma \pi^2 \rho_0 \zeta}\right)^{\frac{1}{3}} \int I^{\frac{2}{3}} dt = r^2 \tag{10}$$

Tom Martin then uses equation (10) to compute the plasma resistance R as:

$$R = \frac{L}{\sigma \pi r^2} \tag{11}$$

Where L is the gap length, and r^2 is determined from equation (8) based on time-dependent current. This resistance is then used to determine the behavior of switchgear, predicting current rise-times and run-times.

Thomson scattering measurements performed at the P3SC were performed to examine the behavior of the switch at atmospheric conditions [9], [10]. These measurements demonstrated that new, low-impedance switches could deviate from the Martin-Braginskii model. Particularly, a notable increase in electron temperature occurs during the rising edge of the current pulse, which is not normally predicted. These measurements seen in Figure 4 give insight into the state of the plasma in the switch. High electron temperatures of ~25 eV indicate that much of the gas in these switches is fully ionized even at low operating voltages (~12 kV), creating a large amount of possible recombination pathways for the ions to take while cooling. This is one of the primary reasons SF_6 is used, as it tends to recombine back into SF_6 quickly [27].

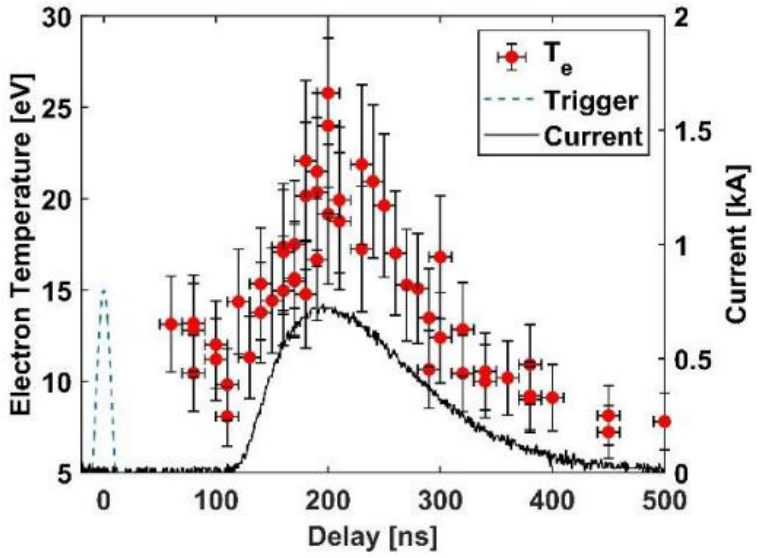

Figure 4: Electron temperature measurements in HV-LTS. Credit : Jacob Gottfried [10].

1.4 Research Motivation

Sulfur Hexafluoride is a dielectric gas with properties desirable for use in high voltage switches systems [11], [28]. With a high dielectric strength, this gas can be used at lower pressures than other gases while still requiring a very high voltage to breakdown [29]. Additionally, SF_6 has desirable arc quenching properties which help quickly interrupt the current by extinguishing the arc [4]-[6]. This quenching property also limits equipment damage and makes the operation of the switch safer for personnel [32]. SF_6 also tends to decompose into byproducts such as SF_4 and S_2F_{10}, which then recombine back into SF_6 after the arc is quenched, restoring the same insulating capability [27]. While SF_6 provides significant performance benefits, it is also very expensive, and faces major supply chain challenges, particularly given the large quantities needed for modern high voltage and pulsed power systems. The need to reduce SF_6 usage is a pressing issue for the continued development and operation of such systems. Currently, no solution exists to fully eliminate this gas from modern high voltage applications.

Efforts to find alternative gases to SF_6 are ongoing, but more research is still needed, as many of these gases are expensive and challenging to implement [11]-[14]. Another possible solution is to use zero-air (synthetic air nominally composed of 79% N_2 and 21% O_2, with trace impurities typically below 1 ppm total) at higher pressure to insulate systems [37], [38]. However, this also creates problems due to the high-pressure requirement, poor arc quenching properties, and poor reliability over time [39], [40]. Thus, a mixture of zero-air and SF_6 is being considered to bridge the gap. Ideally, this would not require significant equipment redesigns. A mixture may be able to reach sufficiently high voltages with less increase in operation pressure when compared to a pure zero-air counterpart [29]. Currently, there is limited data available on these mixtures to support new switch designs. This research aims to address that need.

1.5 Thesis Objectives

The main objectives of this work are as follows:

- Develop a testing method to isolate dielectric gas behavior in current switch testbed.
- Alter switch testbed to minimize losses and accommodate future measurements. This consists of alterations including:
    - Replacement of SF_6 submersion tank with an oil submersion tank.
    - Alteration of switch housing to accommodate higher pressure operation, including creation of pressure management systems for gas mixing and filling.
    - Voltage measurements from power supply mirror with accurate calibration using a Fluke high voltage probe.
    - Implementation of automated breakdown, pressurization, and data collection for long data sets.
- Use the adjusted testbed to collect Paschen data for various mixtures of SF_6 and zero-air.
- Perform long-term, unpurged breakdown measurements to examine gas behavior over many breakdown events with Weibull analysis.

The outline of this thesis is presented chronologically, beginning with initial design work to adjust the switch testbed at CSU in preparation for the intended experiments. Chapter 2 describes much of the work done to increase the testbed capabilities, including experimental procedures. Chapter 3 presents results and analysis of data regarding SF_6 and zero-air mixtures, as well as long-term data examining gas behavior and reliability. Chapter 4 presents conclusions and discusses possible future work.

2. Experiment Design and Laboratory Development

2.1 Methodology

Accurately measuring the breakdown voltage for a given gas or gas mixture involves several challenges. Notably, the breakdown voltage is not solely dependent on the gas species, as seen in equation (1). There are several variables which must be kept as constant as possible between tests, to ensure the gas behavior is being isolated, and the system performance is not majorly dependent on another variable. For the performed experiments, a constant gap spacing of 3.5 mm was maintained between the electrodes at all times, fixing the d variable. Pressure was an independent variable, which would vary anywhere from atmospheric pressure to approximately 180 kPa. Finally, this leaves the A, B, and γ variables. A and B are constants associated with the individual gas species and therefore change depending on each examined mixture. However, γ is primarily dependent on the electrode material, which is not changing.

With every breakdown event, energy will be deposited into the electrode faces, this could cause changes in the surface chemistry and thus, γ. To combat this, several options were considered, including the design of a switch with rotating electrodes, which change the surfaces after every shot. However, due to time constraints this was not manufactured, and a conditioning process was instead used to maintain relatively constant surface conditions. The conditioning of electrodes for high-voltage spark gaps is a well-established process which has been proven to be reliable [41], [42].

Measuring the voltage and current of the switch closure transiently was considered, but was ultimately not performed, as only the voltage prior to breakdown was needed. Thus, the

measurement of the breakdown voltage was determined by using a calibrated mirror output from the power supply. The voltage was very slowly ramped, to ensure the system did not overshoot the breakdown event. Using LabVIEW peak-finder, the maximum voltage prior to breakdown was collected. The transient electrical measurements considered involved the usage of derivative monitors, such as a B-dot or D-dot probe. A current viewing resistor (CVR) was also considered but was not implemented. A CVR is quite simple, having a highly calibrated, known resistance, one uses Ohm's law and the measured voltage to determine current.

2.1.1 – Derivative Monitors

Derivative Monitors have been used by the Pulsed Power community for many years to accurately measure transient voltage and current pulses [43]. Based on the self-integrating Rogowski coil, derivative monitors measure the changing electric or magnetic fields that are creating during a current pulse. Thus, they tend to be non-intrusive and can safely measure very large voltages or currents without damage [44]. Two types of derivative monitors were considered for use, a B-dot probe for current, and a D-dot probe for voltage.

A B-dot probe measures the changing flux of the magnetic field by use of a single-turn conductor parallel to the magnetic field. In practice, B-dots are constructed by inserting a single loop coil in an insulation medium such as epoxy, this core is then placed inside of a conductive shell. The loop and shell are then linked to a coaxial cable by an SMA connector, which is connected to an integrator, and then to an oscilloscope which measures the integrated voltage [43]. By Ampere's law, the B-dot experiences an induced electromotive force (EMF) as the current pulse creates a changing magnetic field [45]. This EMF creates an induced voltage which corresponds to the change of field seen by the flux loop, and this voltage is related to the current being measured. Typically, the output of the probe is then sent to an RC integrator. This probe must then

be carefully calibrated against a known current pulse [46]. After the calibration, one must align it carefully to the new measured system, to maximize the magnetic field seen by the probe.

A D-dot probe measures the changing flux of the electric field by using a capacitive coupling of a conductive plate on the probe, to the measured system. The D-dot is effectively an electric-field-coupled probe which measures the change in electric flux density at the surface of a conductor, to represent voltage [47], [48]. The construction of a D-dot probe consists of a conductor, such as a flat plate or coaxial shell, inserted into an insulating medium such as epoxy. This core is then inserted into a conductive shell, and the probe is linked to a coaxial cable by a SMA connector. The coaxial cable connects to an integrator, and then to an oscilloscope which measures the integrated voltage. As the voltage in the pulse changes, the electric flux density creates a changing capacitance and induced voltage. This change in voltage is typically sent to an RC integrator and can be used to measure the actual voltage change in the system. This probe must be carefully calibrated against a known source [49]. In similar fashion to the B-dot probe, the D-dot must then be carefully aligned to maximize the electric field seen by the probe. A D-dot probe with an RC integrator can be seen in Figure 5.

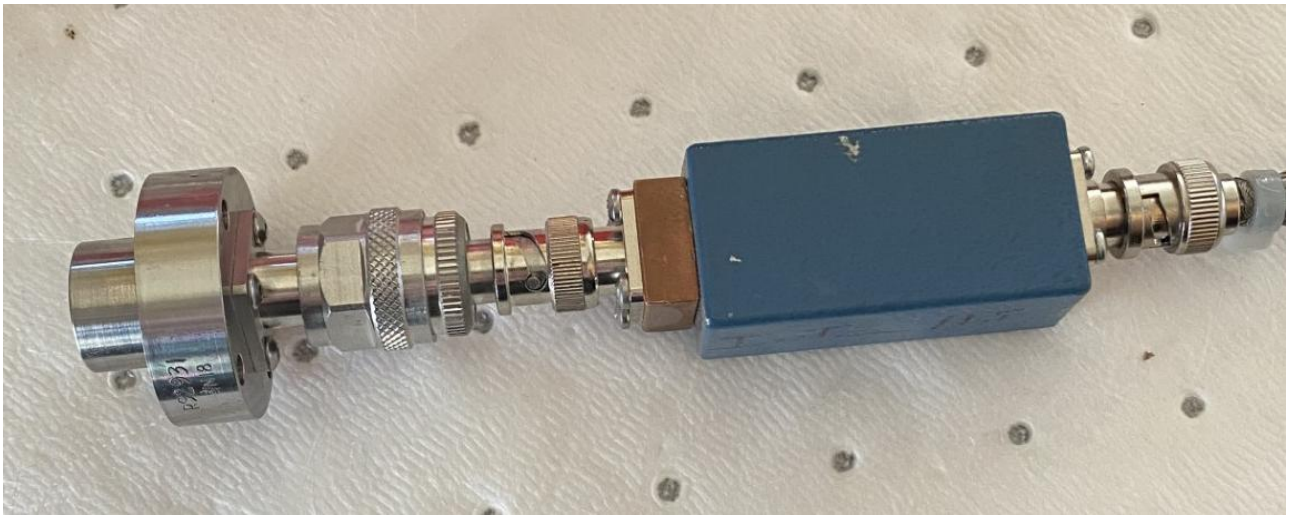

Figure 5: D-dot probe with RC integrator.

These probes can produce very high-quality transient measurements for fast events in high voltage pulsed systems. However, they are challenging to manufacture, calibrate, and install. For this work, a B-dot probe was used to examine the current pulse of the switch in a non-calibrated fashion. This was done to ensure the aqueous load resistor was tuned to a proper matched impedance with the system. All other experiments required measurements of voltage immediately prior to switch closure, which derivative monitors are not able to detect. Thus, a simple resistive probe, and the mirror output of the charging power supply were used to measure breakdown voltages. The inclusion of derivative monitors would certainly be helpful to better diagnose switch performance, but this work was not continued as it was not necessary. In fact, inclusion of such probes could possibly complicate data collection, by introducing field enchantments near the switch and creating additional loss mechanisms.

2.2 Rotary Switch Development

To better isolate the switch performance from electrode surface changes, a new switch design was created at Sandia National Laboratory during a summer internship (Figure 6). The switch was originally intended to maintain optical access, to enable laser triggering and optical measurements. However, due to funding and time constraints, the switch was never fully implemented at CSU. In this switch system, the cathode and anode were placed on spindles linked to stepper motors. After each closure event, a spot size determined from the Martin-Braginskii model would be considered to be damaged [1], [9], [10]. The electrodes would then be rotated, presenting an un-damaged surface before each shot. This would guarantee that every breakdown event has a nearly constant γ, as the material has not changed between events.

This switch was partially manufactured, and several components were tested at CSU. Including testing of the rotary mechanism, electromagnetic pulse testing of the motors, and

pressure testing of prototype 3D-printed vessels. Motor testing demonstrated that stepper motors in close proximity to the switch with fully grounded enclosures could successfully operate after several hundred switch closures. These closure events were at ~20kV, with the motors placed ~5 cm from the electrodes. Hydrostatic pressure testing of additively manufactured pressure vessels, made of durable resin, were successful. The vessels did not fail until twice their designed operating pressure. Such results support the possibility of future experiments on new switch topologies which are independent of electrode surface characteristics for relatively low manufacturing cost.

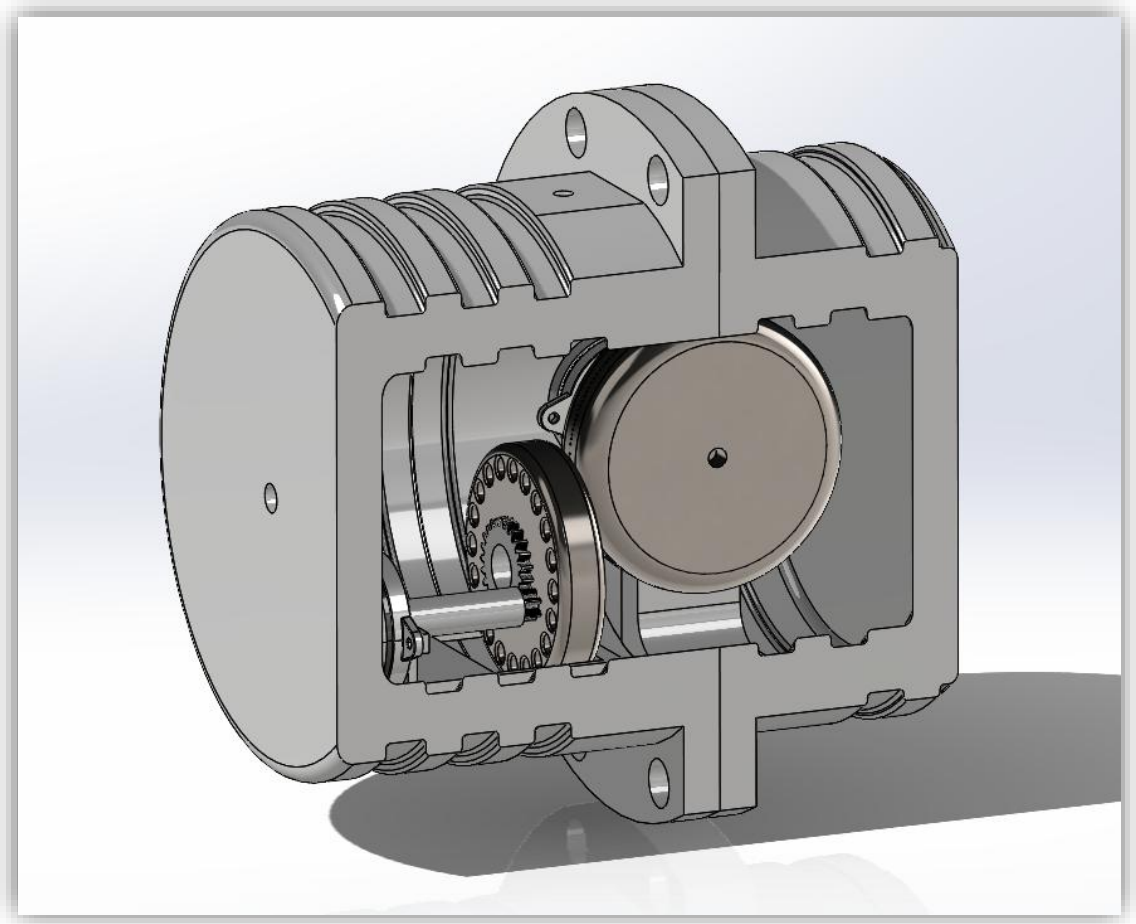

Figure 6: Rotary switch prototype model.

2.3 Experiment Alterations for Breakdown Measurements

The P3SC was originally designed such that most of the electrical components exposed to high voltage were submerged in a large tank, filled with SF_6. A gas was used rather than oil, to accommodate optical diagnostics. However, the system experienced high losses due to suspected corona discharge from the switch body to the grounded Faraday cage around the SF_6 vessel. These losses would cause changes in measured breakdown voltage and would not be sufficient for intended future experiments. The system was manually controlled, with all pressure, voltage, and measurement systems needing to be manually adjusted for every experiment. The intended work for this thesis required the system to be changed, to minimize losses and improve data collection speed. As seen in Figure 7, an oil vessel was created to submerge the tank and insulate the switchgear. This vessel was filled with Shell Diala, a powerful dielectric transformer oil well suited for this type of application.

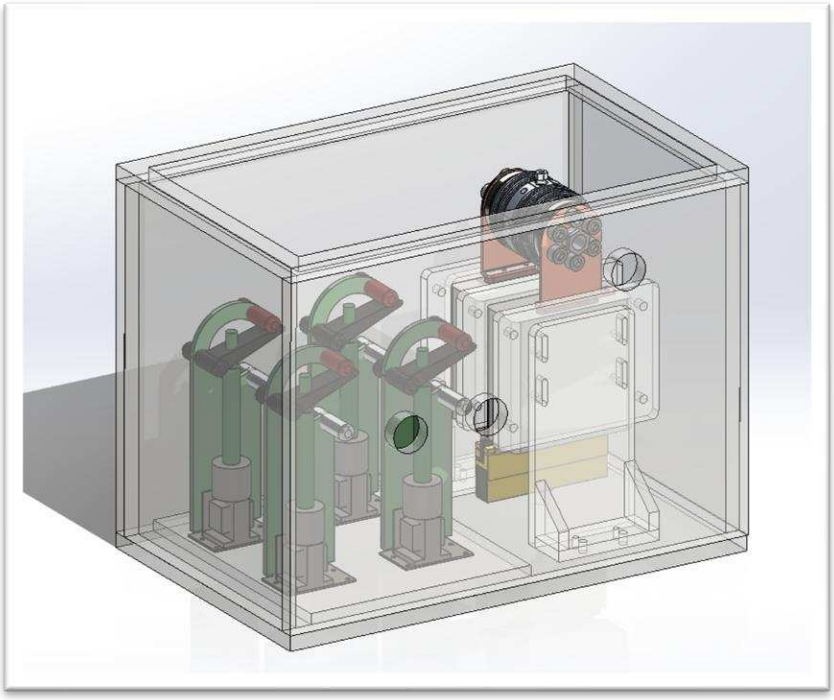

Figure 7: Model of transformer oil vessel with switchgear.

2.3.1 Electrical

The P3SC operates a simple circuit consisting of a negatively polarized Glassman WK high voltage power supply (PS/WK125P5.0-11), linked to a set of two Ross 40kV-Air relays, which are normally closed and ground the system. The relays are connected to an aqueous copper sulfate charge resistor, to protect the power supplies from reflections during switch closure. The charge resistor is then connected to a 100 kV, 20 nF liquid capacitor. The top of the capacitor is then attached to the cathode side of the switch, which consists of two stainless steel electrodes with flat faces spaced 3.5 mm apart within a Delrin pressure chamber (Figure 8). The anode side of the switch is then connected to a tunable aqueous liquid resistor acting as a load, filled with a solution of sodium chloride and deionized water (DI water). This resistor can be tuned by increasing or decreasing the salt content in the DI water. For experiment operation, this resistor is tuned until the load is impedance matched [9]. Finally, this resistor is connected to ground, along with the other side of the main capacitor. All connections were made using 2-gauge solid copper wire, or solid copper bus plates.

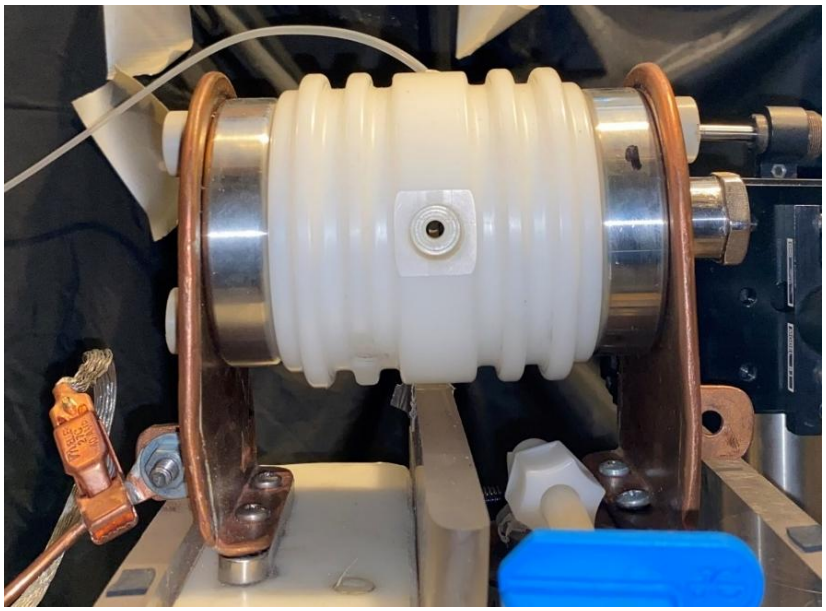

Figure 8: HV-LTS setup with Delrin enclosure.

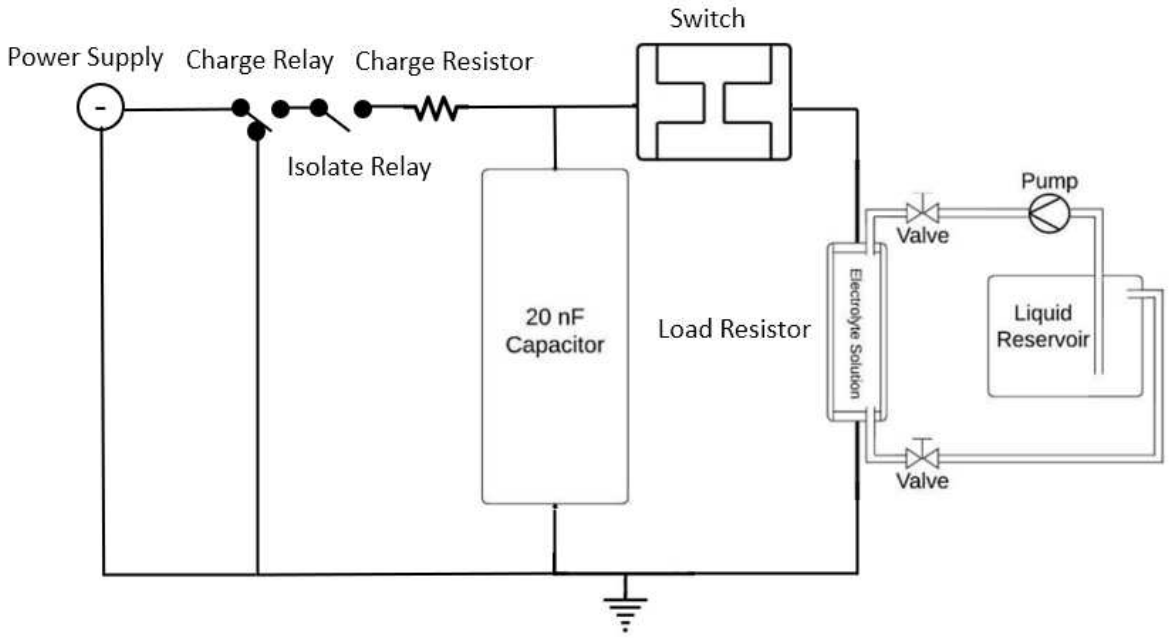

Figure 9: Switch electrical schematic with tunable load resistor.

During operation, the relays are opened, and current is allowed to flow into the capacitor. The voltage in the capacitor slowly rises, limited by the power supply to 0.1 mA to prevent overvoltage and incorrect measurement of the breakdown voltage. Eventually, as the switch approaches the required voltage for breakdown, which depends on the set gas mixture and pressure. The gas rapidly ionizes, forming a plasma, and the capacitor quickly discharges the stored voltage across the gap. The load resistor then accepts the voltage pulse, and the voltage is discharged to ground, the complete circuit can be seen in Figure 9. The plasma is then no longer sustained as the potential across the gap falls, and the switch re-opens. The capacitor then begins to charge again, and this process is repeated until the relays are closed. Liquid resistors are used in this application as opposed to traditional, solid ones. The joule heating caused by closure events is quite high, and many resistors would fail after several breakdown events. Liquid resistors are capable of accepting far more energy, due to their high specific heat capacity, precision, and longevity [50]. All switch components can be seen in Figure 10.

Figure 10: Deconstructed high voltage switch with electrodes and aqueous load resistor.

Significant efforts were made to shield the lab from intense electromagnetic interference during switch closure. Such interference would prevent accurate measurement of the voltage and would create issues with automated systems. Originally, a single Faraday cage made of brass mesh was added around the oil tank, but notable interference was noticed in computer systems used in the lab. A second cage was added around the tank, and a third cage was added around the room the switch was located in. Additional stainless steel mesh shielding was added to various cables connecting the computer and data acquisition (DAQ) systems to the rear of the power supply for measurement. The Faraday cage can be seen surrounding the oil vessel in Figure 11.

Figure 11: High voltage switch experiment with Faraday cages.

To further reduce losses in the system, the second set of relays which were no longer operated were removed. These relays provided an additional path to ground and created a possible loss pathway. The wiring for these relays was also removed, and the single set of relays was tested to ensure that they closed and opened properly, including in the event of an emergency shut off.

2.3.2 Pressure

The P3SC was originally designed for single-gas pressurization, and most experiments were to be run at a set pressure for an entire experiment. Later, the switch was run without any pressure for better optical access [10]. Given the current work was intended to examine breakdown voltage at various pressures, the system needed substantial redesign to accommodate the changes. Mainly, this included the addition of gas mixing capabilities, pressure measurement, and more

sophisticated pressure controls. Originally, the system was entirely manual. Original attempts to use the manual system for pure gas measurements were very laborious, and time consuming, further emphasizing the need for a system redesign.

The switch was originally pressurized with an old valve system, connected to the original SF_6 submersion tank, which was removed as the new oil tank was added. A new system was designed, this time with the addition of a gas mixing tank. This tank would allow for the creation of a high-pressure mixture of gases, by using Dalton's law of partial pressures. Then, the mixing tank would act as the primary pressure source, ensuring the switch volume was filled with the correct mixture for every operating pressure. The complete pressure schematic can be seen in Figure 12.

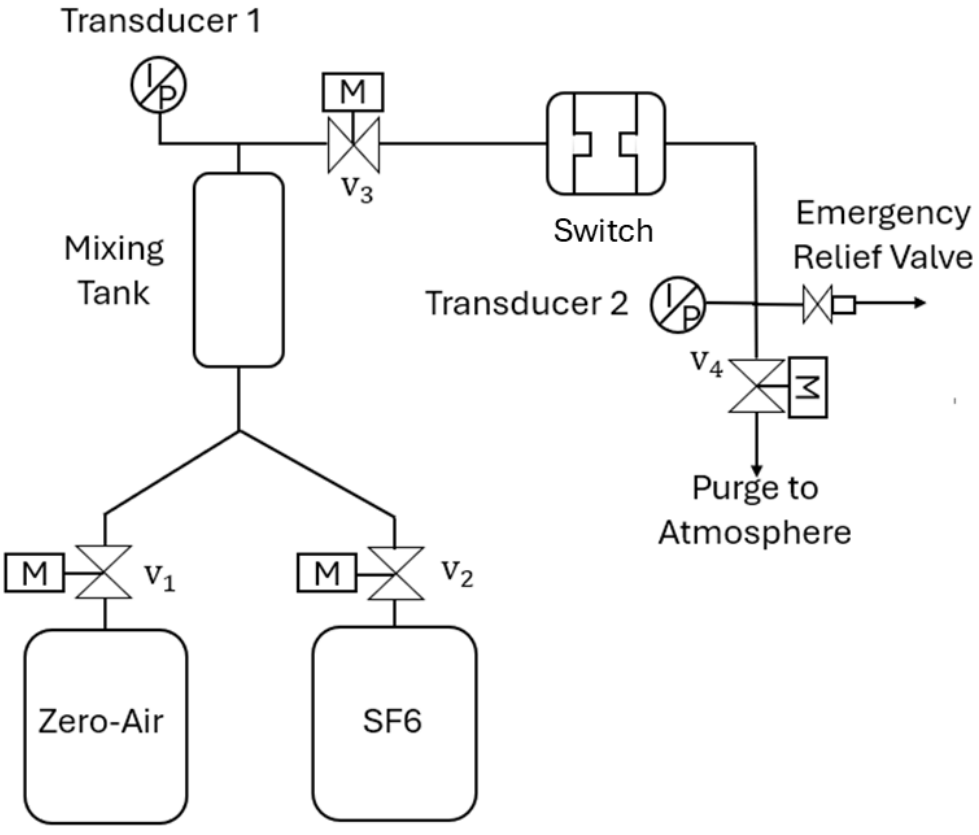

Figure 12: Automated pressure system schematic.

All pressure lines outside of the primary faraday cage are made of stainless steel, with Swagelok connections sealed with Teflon tape. The pressure lines into and out of the switch body are made of polyethylene tubing, as conductive steel tubing would act as a path to ground. Leak tests show that there is very minimal leak in the system, with no pressure drops being recorded over an 8-hour test period.

To properly fill the switch with the correct mixture, there is a specific order of operations which must be followed to ensure that the volume is purged and filled with the proper gas. The order of operations is as follows:

1. Open zero-air tank and adjust the regulator to desired partial pressure.
2. Open SF_6 tank and adjust the regulator to desired partial pressure.
3. Open zero-air valve (1), mixing tank valve (3), and purge valve (4). Flow zero-air to purge system for 2 seconds.
4. Close zero-air valve (1), mixing tank valve (3), and purge valve (4).
5. Open SF_6 valve (2), bring mixing tank to correct partial pressure measured by transducer (1).
6. Close SF_6 valve (2), allow pressure to stabilize.
7. Open zero-air valve (1), bring mixing tank to correct total pressure measured by transducer (1).
8. Close zero-air valve (1), allow pressure to stabilize.
9. Open purge valve (4), open mixing tank valve (3), purge system with proper gas mixture for 2 seconds.
10. Close purge valve (4), pressurize until transducer (2) is at desired operation pressure.
11. Close mixing tank valve (3), allow pressure to stabilize.

12. Run experiment, after completion, open purge valve (4), and open mixing tank valve (3) until system returns to ambient condition.

2.3.3 Automation

To increase the experiment speed and minimize manual operation, an automated system was developed in LabVIEW to pressurize, energize, and measure the breakdowns of the experiment. Two Honeywell PX2AN1XX030PAAAX pressure transducers are used to monitor the pressures inside of the mixing tank and inside of the switch volume. The transducer signal is then used to feed back into the LabVIEW program by means of a NI-USB6003 data logger, allowing for the user to set a desired test pressure. The LabVIEW then follows the correct order of operation as listed in section 2.3.2, by operating three iQ Tesla 2-way valves. Once pressure conditions are correct, the only remaining manual input required for the tests to proceed is the opening of the primary charge relay. The LabVIEW program then continuously measures the voltage in the system, by means of a mirrored output on the rear of the power supply. Eventually, the breakdown occurs, and the voltage rapidly drops. The data stored by the LabVIEW program is sent to a file read by a MATLAB script, which determines the maximum recorded voltage prior to the breakdown event.

2.4 Measurement Methods

To accurately measure the voltages and pressures in the experiment, the systems transducers and mirror output measurements need to be calibrated. Voltage calibration was done by first using a Fluke 80k-40 HV-Probe, attached to a Fluke voltmeter. This probe is accurate to ± 1% in the calibrated range. The meter was first checked using standard prong probes on a known voltage source from an Arduino UNO output. Then, the 80 kV probe was tested on the same

voltage. The 80 kV probe is a 1-1000 voltage divider, and once the voltage was confirmed to be correct, the probe was attached to the top end of the charge capacitor.

The switch was pressurized with sulfur hexafluoride such that the switch did not close and damage the probe during the calibration. The system was then brought to several different operating voltages in a range of 0-60 kV and was held for several seconds at each condition. At each condition, the voltage from the probe and the mirrored voltage from the supply were collected, and a calibration curve was created (Figure 13). The curve is quite accurate with a linear fit, and this test was repeated twice to ensure that the results were repeatable.

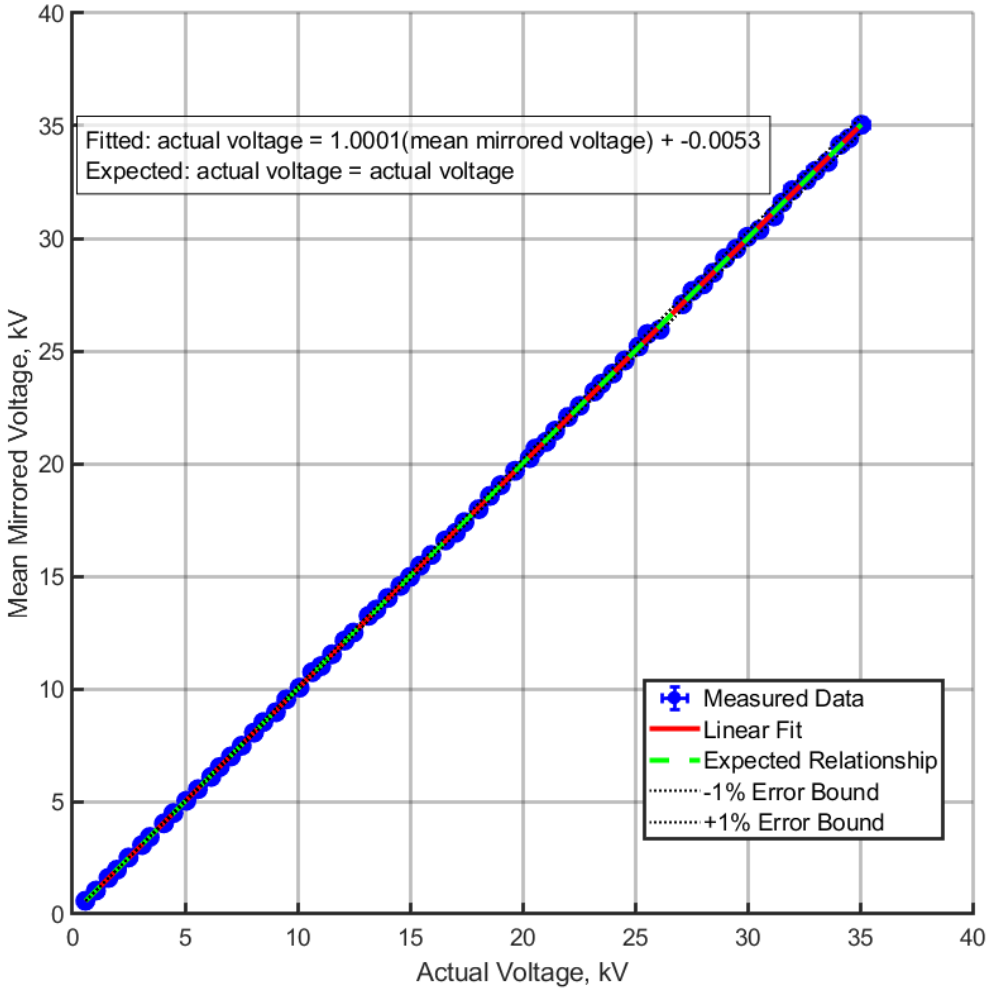

Figure 13: Voltage calibration curve.

The pressure transducers were calibrated in a similar fashion to the electrical probe. First, an Omega pressure transducer which was already calibrated and checked against an Airgas 224 dial pressure gauge on the regulator from the zero-air tank, was attached to the pressure lines. The pressure transducers were attached on the same line, as close as possible to the calibrated transducer to minimize any line losses. The zero-air tank was then opened, and the pressure was swept through several points, and the voltage output of the transducers was logged to create the calibration curve. The created calibration curve is shown in Figure 14.

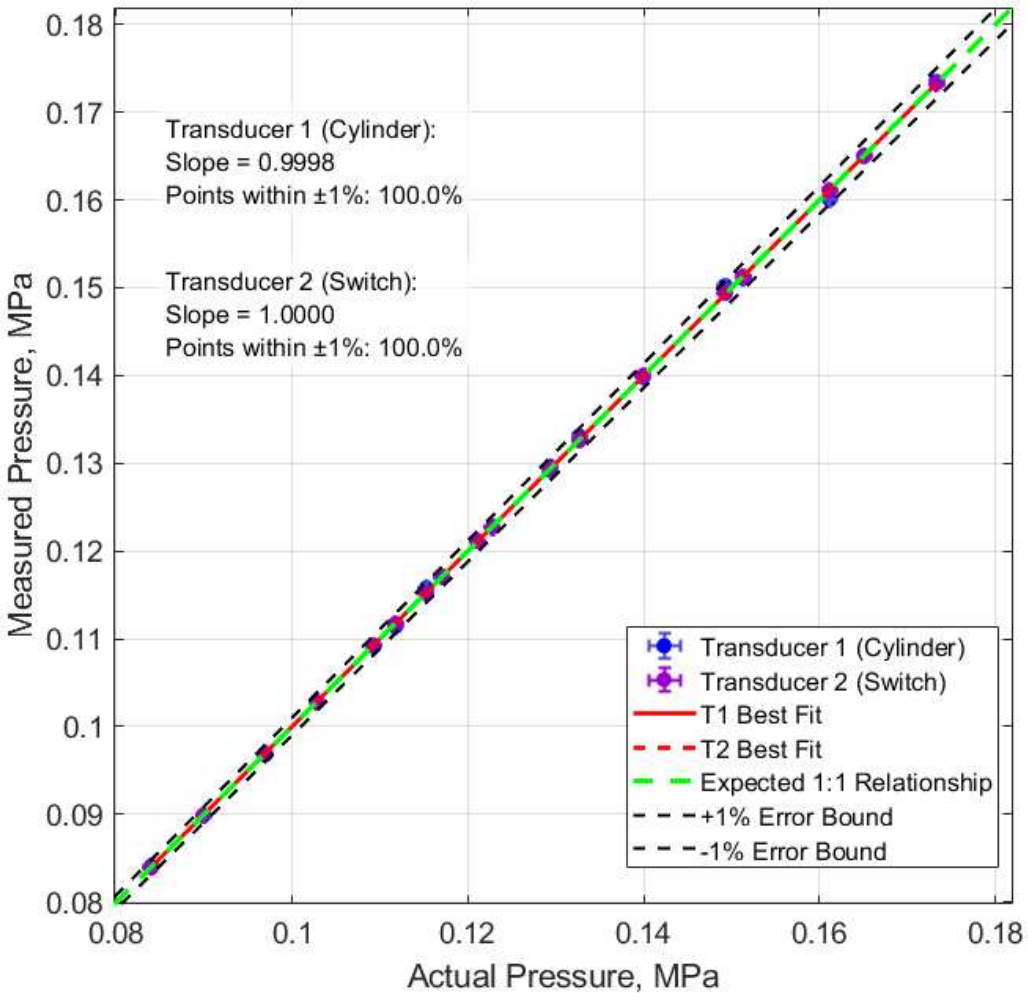

Figure 14: Pressure calibration curve.

To identify the point at which breakdown occurs, the live voltage data is analyzed with LabVIEW peak detector, this peak detector identifies the maximum peaks in the voltage trace. To identify when a breakdown occurs, a voltage threshold is set at a value close to the expected breakdown voltage for the gas or gas mixture. Then, when a breakdown occurs, the falling edge of voltage signal informs the LabVIEW to save the peak voltages in a file. From these peak voltages, a MATLAB script is then used to identify the maximum values for each closure event. These maximum values are then considered to be the breakdown voltages, as they are the highest voltage seen by the system prior to switch closure. An example of a detected breakdown event and voltage trace is shown in Figure 15.

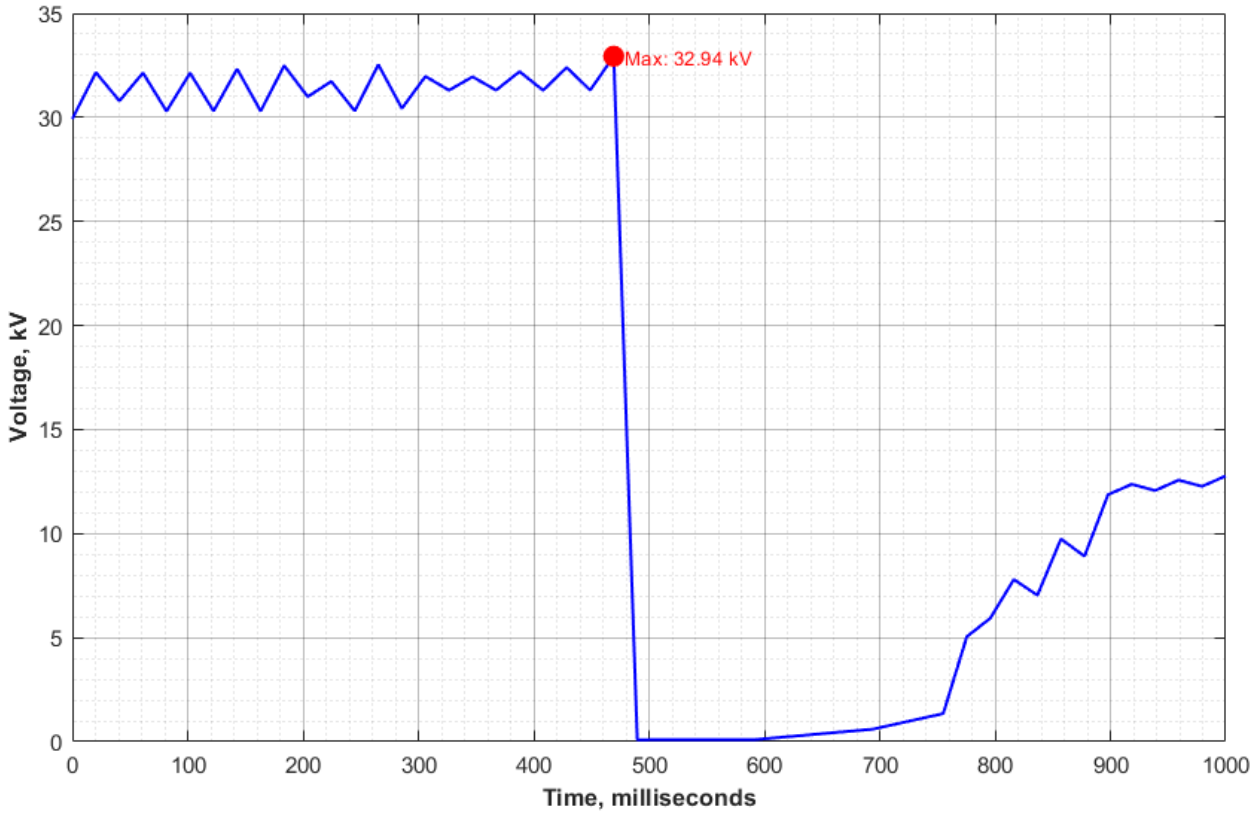

Figure 15: Voltage measurement during breakdown event.

2.4.1 – Noise Reduction

A major issue with the automated system was the high noise created during system operation. Such noise was significant, on the order of 1000 V from the calibrated and scaled mirror output. Physical mitigation of the noise was first attempted before any filtering of the noise was considered. This included the removal of all unused electrical systems and verification of a common ground for all systems. The installation of several Faraday cages around the switch oil vessel, all connecting lines, and the DAQ. The DAQ was eventually moved in its entirety to a stainless-steel metal safe, which was grounded to provide more shielding. Such adjustments did reduce the noise seen in the system, but noise was still too high to be permissible.

To better analyze the source of the noise, a Fast Fourier Transform (FFT) was performed to the live data collected by the DAQ from the power supply mirror (Figure 16). The FFT algorithm was included in the LabVIEW software package. Results from the FFT demonstrate that nearly all noise was coming from a 60 Hz source, or from the DC (0 Hz) output from the power supply. The DC signal was all that should be measured, so efforts to specifically target the 60 Hz noise were taken. The 60 Hz noise from wall-outlet noise, this was determined by using an emergency stop button in the lab, which physically disconnects the system from all wall-outlet sources [1]. A major amount of noise at 60 Hz was then seen in the live output of FFT as this connection was switched on and off. In the United States, wall outlet runs at 60 Hz standard, which confirmed that the noise was likely coming from this connection.

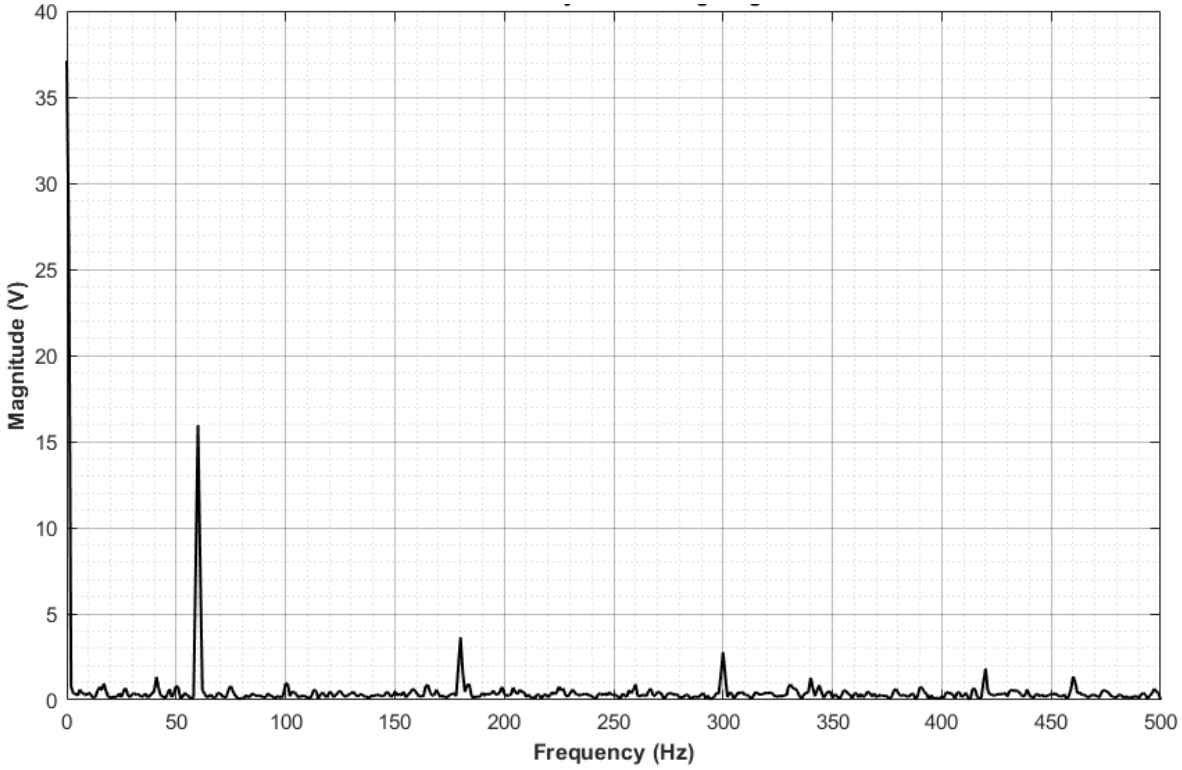

Figure 16: Fast Fourier Transform (FFT) plot.

Since this noise was identified to come from this source, a data filter was implemented. This filtering is valid, as it is only coming from the single identified source. The noise does not contribute to any real signal from the power supply, and removal of the noise would not impact the real voltage being supplied to the switch. A type I Chebyshev filter was selected to remove the 60Hz signal. This type of filter was selected as it has very sharp cutoff for the frequencies outside of the passband, which enables the targeted removal of non-DC signal. The passband was set to 0-0.01 Hz, to permit only DC signal to pass the filter. The addition of the filter greatly reduced the noise in the system, on average by ~500 V, improving the accuracy greatly. The unfiltered voltage and filtered voltage are compared in Figure 17.

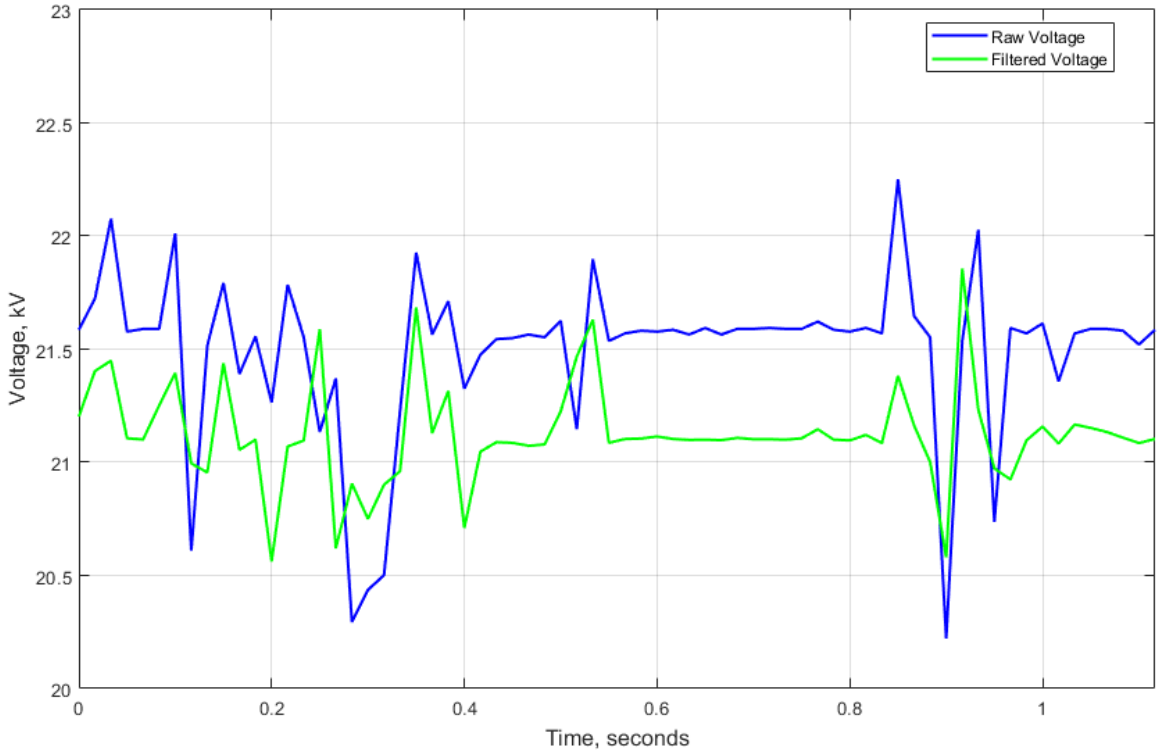

Figure 17: Unfiltered vs. filtered voltage.

3. Results and Discussion

3.1 Paschen Curves of Pure Gases

To ensure that the system was behaving as expected, Paschen curves of pure SF_6 and pure zero-air were collected over a pressure range of 83 kPa to 172 kPa. The electrodes of the switch were first polished with sandpaper until a 600-grit finish was achieved. The electrodes were then conditioned using the standard procedure outlined in section 2.3.1. The system was then sealed, and the oil vessel was filled to insulate the switch. The system was pressurized to the desired test pressure, and voltage was turned on. The voltage was slowly ramped up by limiting the current to 0.1 mA, until the gas experienced a breakdown.

The maximum voltage at each breakdown event was logged, and the procedure repeated for 10 closures per condition. The measured values were then averaged, and the switch was brought to the next operating condition after purging and refilling the dielectric test gas. These tests were repeated until 5 different conditions were tested. The electrodes were then cleaned, conditioned, and the tests repeated 3 times.

A linear fit was then applied to all of the data to generate a line for each gas. This data was compared to three other tests collected on the switch at an earlier time, to ensure that repeatable behavior was being measured. The residuals of the data were plotted against pd, and against a normal distribution. Each Paschen curve plots the average value of all breakdown events measured at a given pressure condition. The three tests performed are then all plotted in a scatter plot, and the line of best fit is applied to all of the data using a least squares method. Figures 18 and 19 show the created linear fits for pure air and pure SF_6.

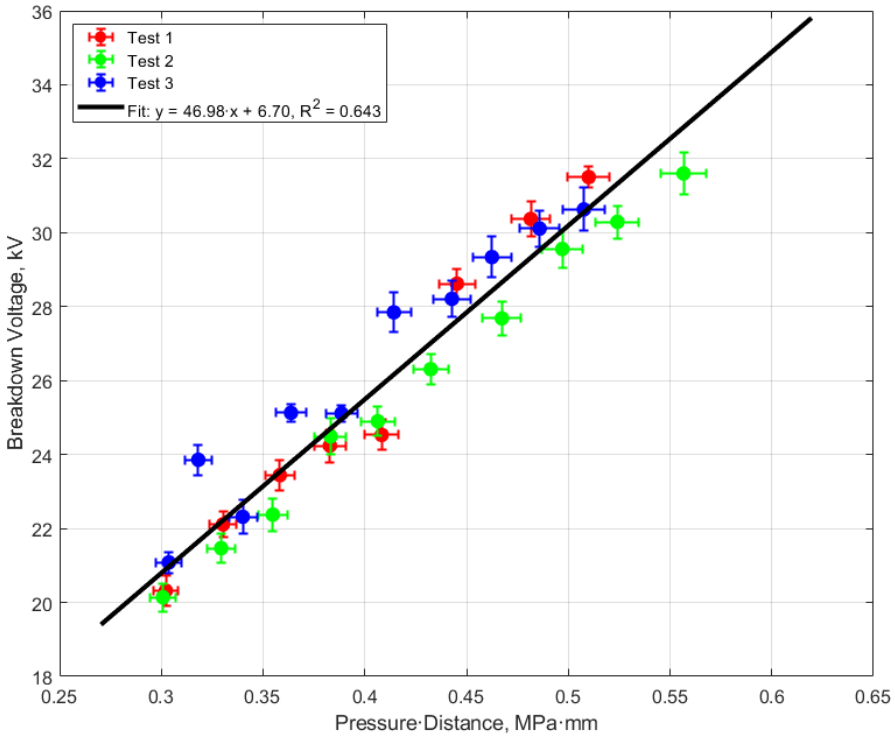

Figure 18: Pure zero-air Paschen curve.

Error bars are provided for both pressure and voltage measurements. The propagated error for voltage was determined by first using the ± 1% error from the FLUKE probe used for creating the calibration curve. The standard error of the mean was then added based on the ten shots per operating condition. An additional ± 6 mV error was also added due to the rated noise from the DAQ. The propagated error for pressure was determined by using the ± 0.08% error from the calibration transducer. Then, the additional rated ± 0.25% error for a Honeywell PX2 series transducer was added, as well as the standard error of the mean and the ± 6 mV from the DAQ.

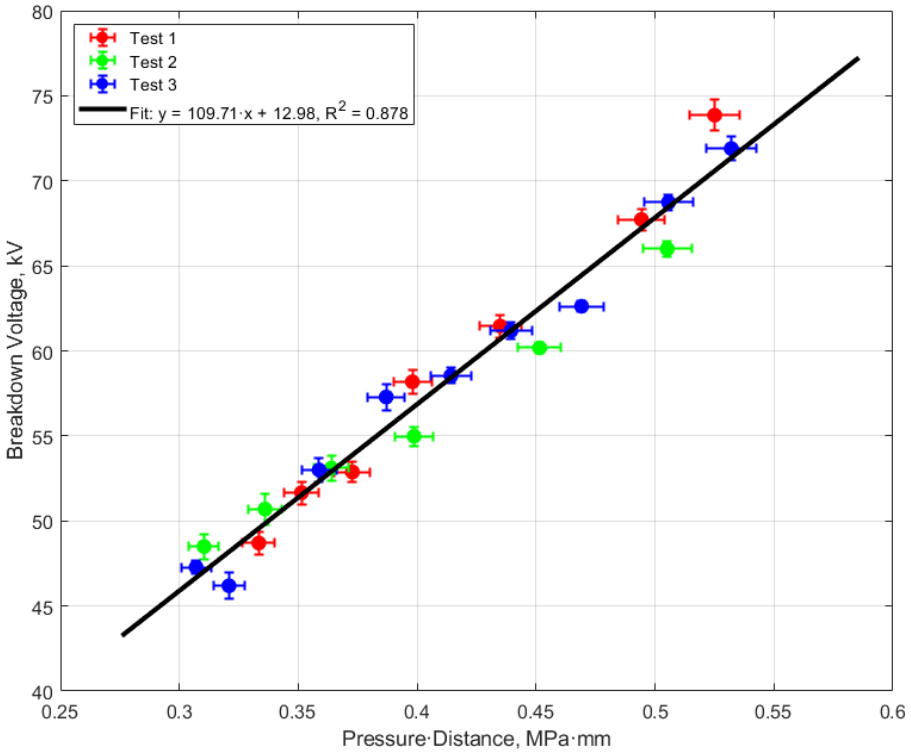

Figure 19: Pure SF_6 Paschen curve.

It is important to note that the standard accepted value of 30 kV/cm for the breakdown of air in atmospheric pressure is not seen in the collected data. Additionally, the slopes of the fitted lines deviate from calculated linear fits of Paschen's law in this pd region. The reason for these

deviations can be determined by examining equation (1). The breakdown voltage is heavily dependent on coefficients A and B.

However, in numerous studies it has been shown that experimental values for A and B can vary considerably between different studies [55]-[57]. In this case, the collected Paschen curves are only valid for this particular switch topology. Other switches with similar spacings have demonstrated some level of divergence from Paschen's Law [54], [55], [56]. The deviations are theorized to be caused by electric field non uniformities, which would alter the A and B coefficients calculated in equation (2). Further analysis of the deviation from theory can be found in section 3.3. The field non-uniformity in the examined switch is likely caused by fringing effects, as the electrodes are nearly flat plates with radiused edges. A cross section of the switch, and the electrodes can be seen in Figure 20.

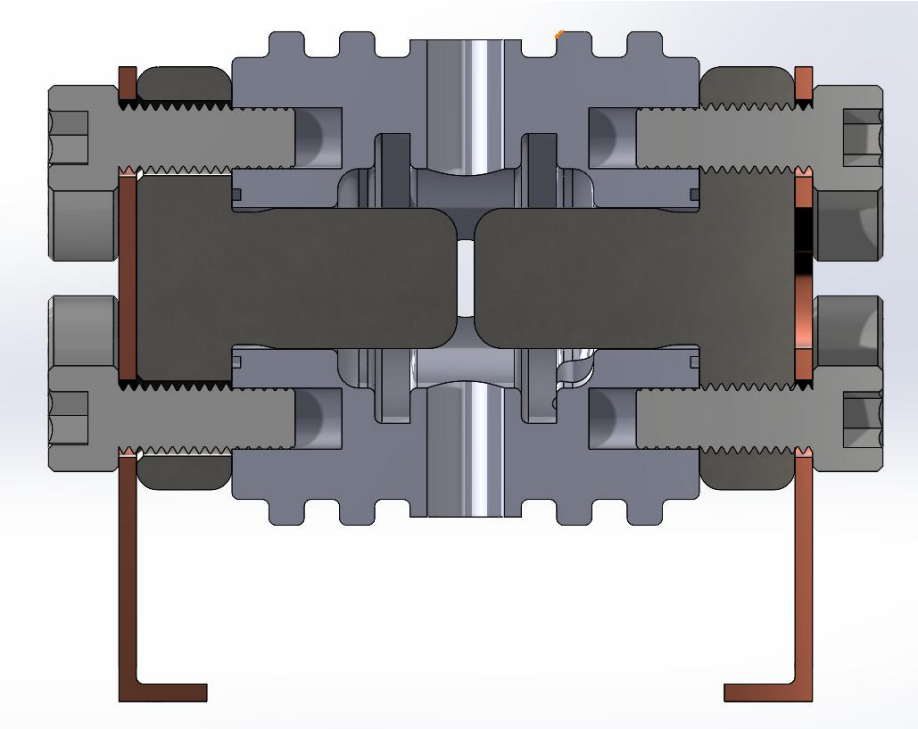

Figure 20: High voltage switch cross section.

3.2 Paschen Curves of Gas Mixtures

To examine the breakdown behavior of gas mixtures of SF_6 and zero-air, three mixtures were tested in the same scheme as the pure gas tests in section 3.1. These mixtures consisted of 25% SF_6 – 75% Air, 50% SF_6 – 50% Air, and 75% SF_6 – 25% Air. All mixtures were tested over a pressure range of 83 kPa to 172 kPa, and their respective breakdown voltages were recorded. Each mixture was tested with conditioned electrodes, for 10 shots at each pressure condition. These tests were all repeated three times per mixture to ensure repeatability. Figures 21-23 show individual Paschen curves for each created gas mixture. A full set depicting all measured Paschen curves is seen in Figure 24.

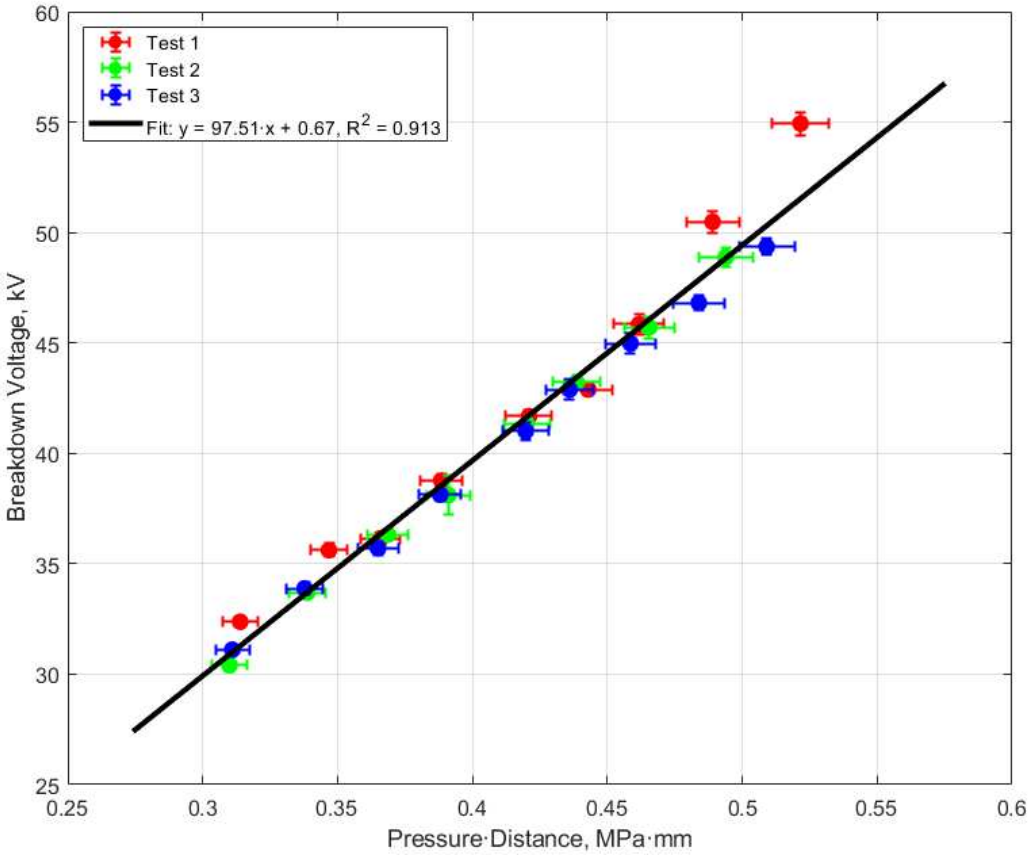

Figure 21: 75% zero-air - 25% SF_6 Paschen curve.

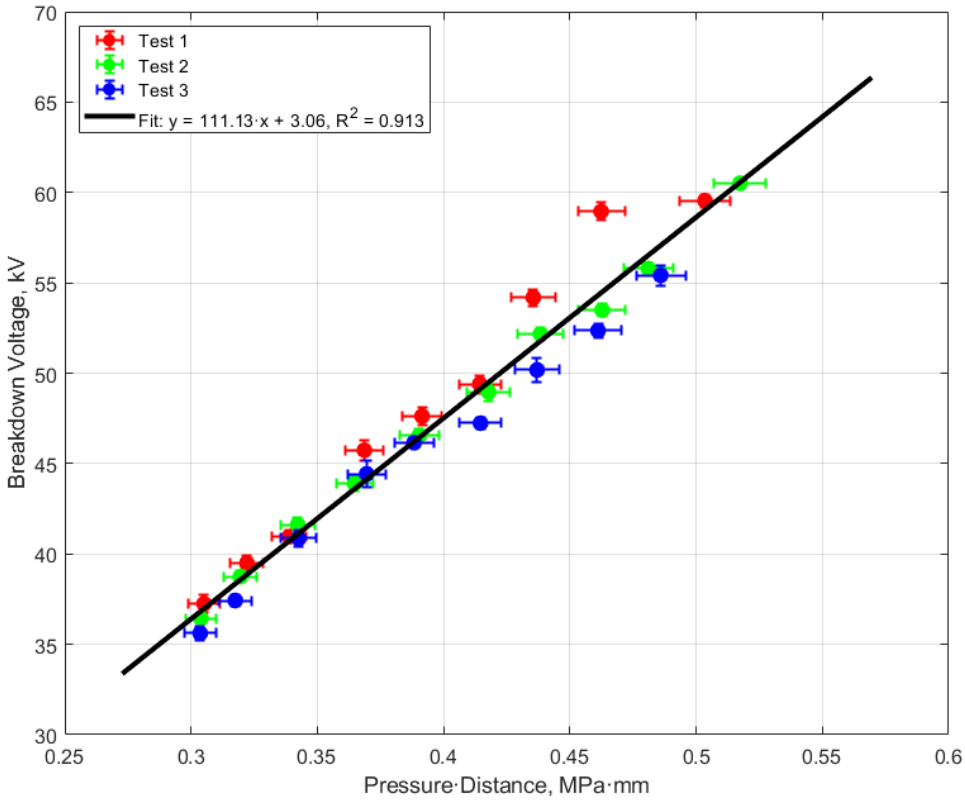

Figure 22: 50% zero-air - 50% SF_6 Paschen curve.

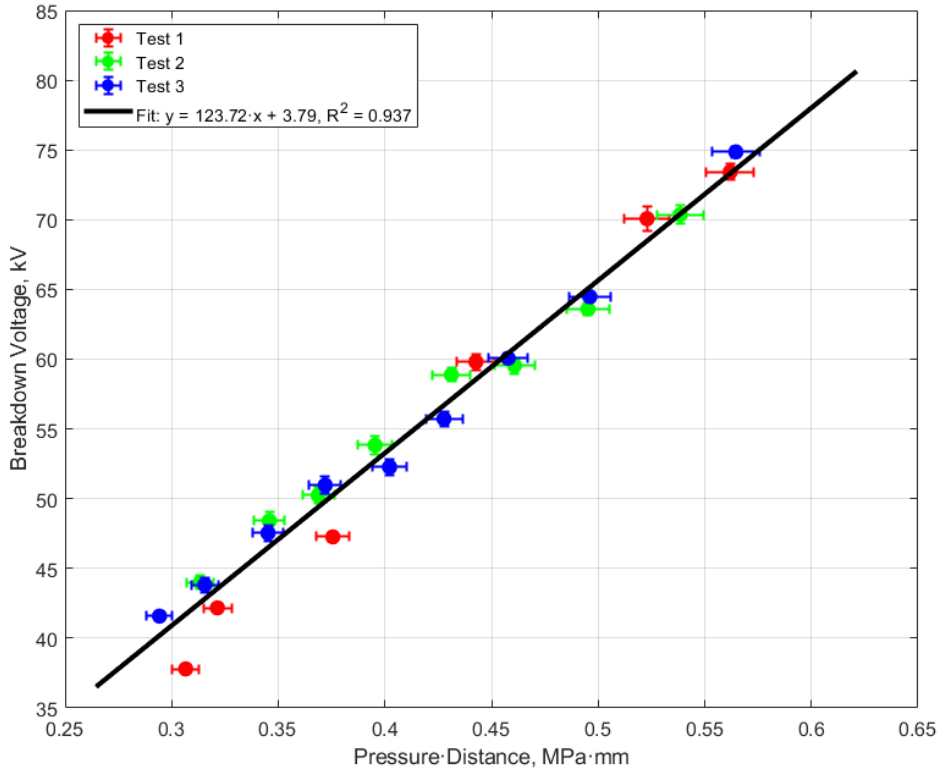

Figure 23: 25% zero-air - 75% SF_6 Paschen curve.

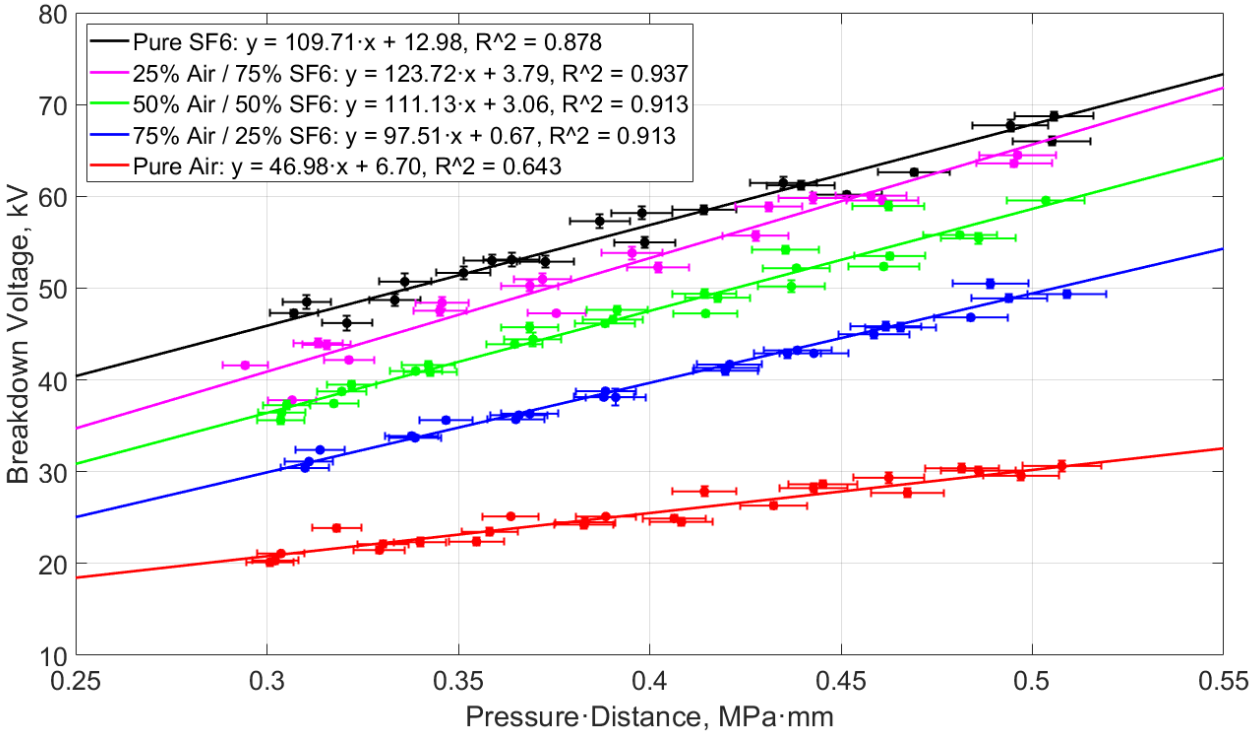

Figure 24: Paschen curves for all mixtures of zero-air and SF_6.

From the results, it is apparent that a small amount of SF_6 in the mixture has a dramatic effect on dielectric strength. The 75% air – 25% SF_6 mixture demonstrates a ~50% increase in breakdown voltage when compared to pure air. This effect becomes less pronounced as the percentage of SF_6 in the mixture approaches 100%. This data is valuable, as it shows possible reduction of SF_6 usage in high voltage switchgear can be achievable, while only having moderate pressure requirement increases. For example, to use a 50% zero-air – 50% SF_6 mixture in a switch designed for self-break at ~50 kV using pure SF_6, the switch would only need to increase the operating pressure by ~0.1 MPa (~1 atm), while reducing their SF_6 usage by 50%. These results show that a mixture of SF_6 and zero-air, and thus a reduction of SF_6 usage, has the capacity to be quickly implemented into switchgear without the need for challenging switch redesigns.

3.3 Linear Approximation and Agreement to Theory

The data presented in sections 3.1 and 3.2 show linear approximations fitted to collected breakdown data. However, Paschen's law is not inherently a linear equation but rather follows an exponential relationship between breakdown voltage and pd. The right-hand side of the Paschen minimum, in high pd regions, can be reasonably approximated as linear, provided that the data does not cover an extremely wide range of pd values [57]. This linear approximation is particularly useful for high pressure switch applications, which fall within a constrained parameter space.

To validate this linear approximation, established literature values of A, B, and γ for air were used to compute the full Paschen's law relationship over the experimental pressure range of 80-180 kPa. The computed theoretical data were then fitted with a linear regression line as seen in Figure 25, and the maximum deviation from the theoretical curve was systematically determined across the entire pressure range. The results demonstrate that the linear approximation deviated by a maximum of only 0.8% from the full Paschen equation predictions across the examined pressure range, thereby confirming that the linear approximation is valid and sufficiently accurate for use in this operating regime.

In practice, the collected experimental data may exhibit deviations from the accepted theoretical values of breakdown voltage for these gases and gas mixtures. Presently, this is assumed to be due to inadequate electric field uniformity in the gap, which is a fundamental assumption used by Townsend in equation (2). The non-uniformity results in values of A and γ which are not consistent across all switch topologies [58], [59], [60]. Additional factors such as surface roughness, field enhancements, or gap contamination may also lead to deviations from the theoretical values.

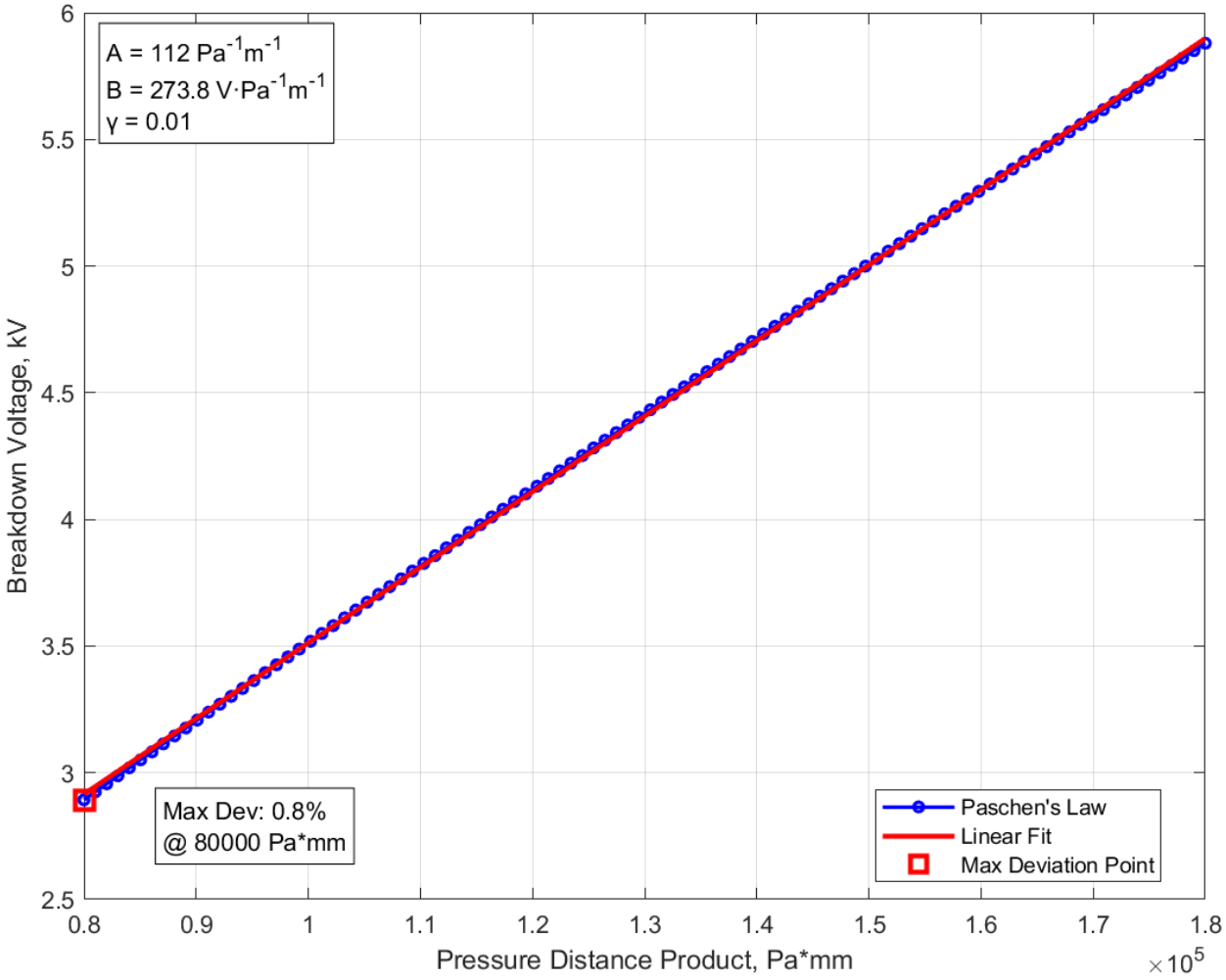

Figure 25: Linear fit of high pd region of Paschen's law with standard A, B, and γ values for air.

Thus, while the data is not sufficient to provide exact voltages for every switch topology and pd region, the general trends still hold, as demonstrated by the strong statistical evidence for linear behavior in the test regions. The R^2 values obtained for each linear fit demonstrate good correlation between the experimental data and the linear model, indicating that the linear relationship accurately captures the underlying physical behavior consistent with this region of Paschen's law. This statistical validation aligns with the theoretical expectation that breakdown voltage should exhibit linear dependence on pressure in the high pd regime.

The validity of the linear fitting method is further confirmed through analysis of the residuals. The residuals between the experimental data and linear fits follow a normal (Gaussian) distribution, which indicates that deviations from the linear trend are random rather than systematic, supporting the appropriateness of the linear model. Additionally, Shapiro-Wilk tests were performed on the residuals between the data and the linear fit of each dataset to evaluate the normality assumption [61], [62]. The typical significance level of $\alpha = 0.05$ was used as the criteria for the test, with the probability values (p) listed in Table 1. Since all p values exceed the significance criteria, the null hypothesis of normality cannot be rejected, thereby confirming that the data can be considered to follow a linear relationship and that the linear fitting method is statistically valid.

Pure Air	75%-25%	50%-50%	25%-75%	Pure SF_6
p = 0.0725	p = 0.1967	p = 0.2181	p = 0.2962	p = 0.3008
$\alpha = 0.05$	$\alpha = 0.05$	$\alpha = 0.05$	$\alpha = 0.05$	$\alpha = 0.05$
$R^2 = 0.643$	$R^2 = 0.878$	$R^2 = 0.913$	$R^2 = 0.913$	$R^2 = 0.937$

Table 1: Shapiro-Wilk test results and R^2 values of linear fits.

Such data should be used to inform the design of switches attempting to switch to a zero-air – SF_6 mixture, but exact values for operation will be heavily dependent on the specific switch properties. This aligns with other works' findings that electrode geometry and gas properties create unique, but consistent Paschen parameters for a given experimental setup [59]. Additionally, the ratio of breakdown strengths between SF_6 and zero-air in the performed experiments has been found to be 2.35 to 1. This ratio closely aligns with previously reported relative dielectric strengths in various studies, suggesting that the system is accurately capturing the physics of the breakdown event despite differences in the absolute measured actual values [63], [64].

3.5 Long Term Measurements of Pure Gases

For many switch applications, the breakdown voltage must be known to a high degree of accuracy. For example, HV-LTS's used in SNL's Z-Machine are charged to a percentage of self-break, i.e., specified percentage of the full breakdown voltage for a given gas, switch design, and pd value. SF_6 has desirable recombination characteristics after breakdown, with a large amount of the products quickly recombining back into SF_6 [27]. This behavior allows for the continued use of a switch, without needing to reset and refill the gas. Conversely, if the gas composition were to change significantly over time, due to repeated breakdown and recombination events, then the breakdown voltage could also evolve. This evolution would complicate or inhibit continued usage of the switch. This chemical stability over time is one of the primary reasons that replacement of SF_6 is so challenging.

To examine this behavior, the switch was filled with a selected gas or gas mixture and then pressurized to achieve self-breakdown in the 40-50 kV range. The system was then sealed, to ensure the gas in the volume was not replaced by new gas over the test duration. Then, the system was repeatedly brought to breakdown over many thousands of closures. This repeated breakdown process may cause the gas composition to evolve over time.

The breakdown voltages were recorded and then plotted versus shot number in Figures 26-29 for various gas mixtures. The data were normalized to the first 100 shots of each set, to establish the baseline behavior for Weibull failure analysis. The first 100 shots were selected because the breakdown voltage remained highly stable in this initial period across all tests, with no observed failures (as discussed in Section 3.7). During this early phase, the gas composition has not had sufficient time to change significantly, representing normal switch operation.

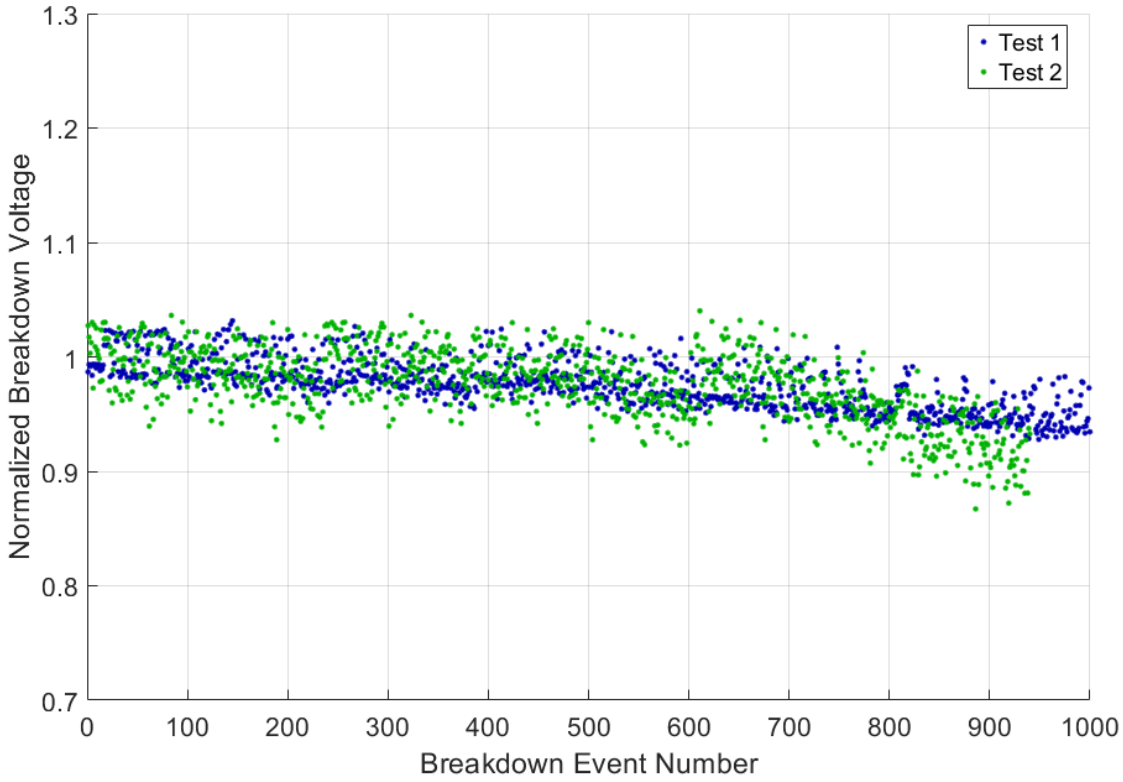

Figure 26: Time-series of normalized zero-air breakdown events.

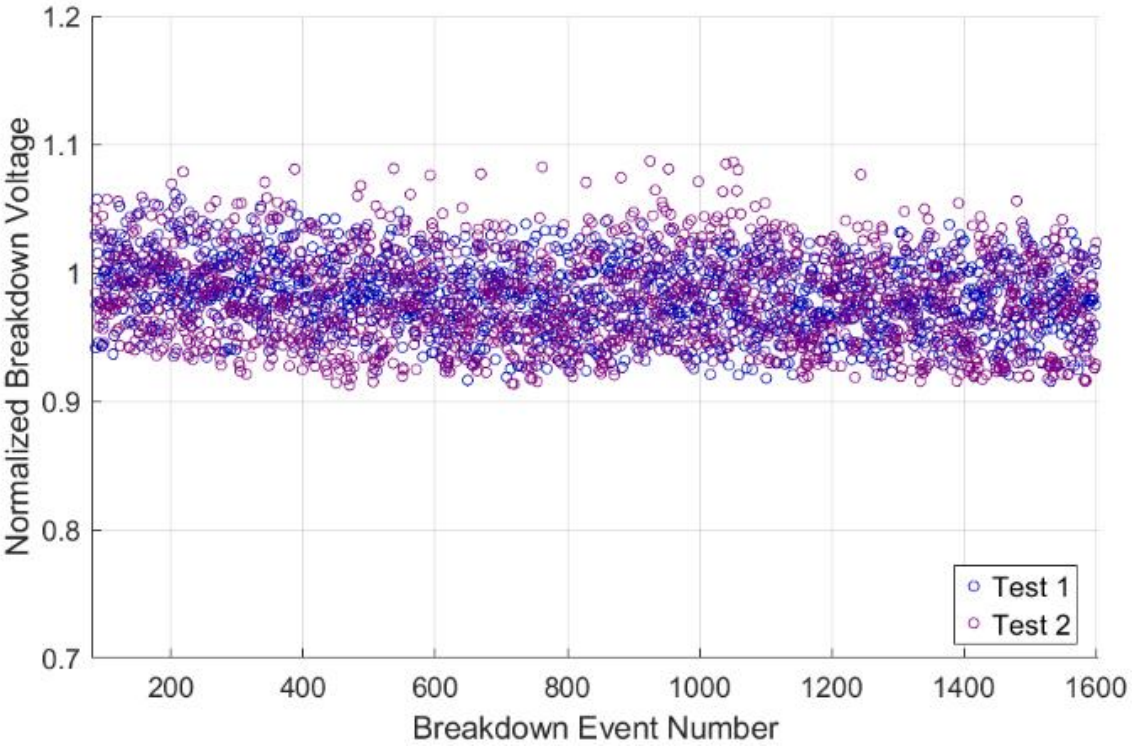

Figure 27: Time-series of normalized SF_6 breakdown events.

As is clearly visible from Figures 26 and 27, the SF_6 exhibits significantly better stability than air with considerably less reduction in breakdown voltage over the test duration. In contrast, zero-air demonstrates a clear degradation in breakdown voltage over time. These results align with expected behavior, as SF_6 recombines into primarily SF_6, and air may recombine into a vast variety of compounds such as O_3, or NO_x which over time change the systems breakdown voltage at constant pressure. These data demonstrate that SF_6 is preferable for long-term use, while zero-air is unsuitable. To confirm that these changing breakdown voltages are caused by gas recombination processes, a dataset of pure nitrogen was also run in the same conditions.

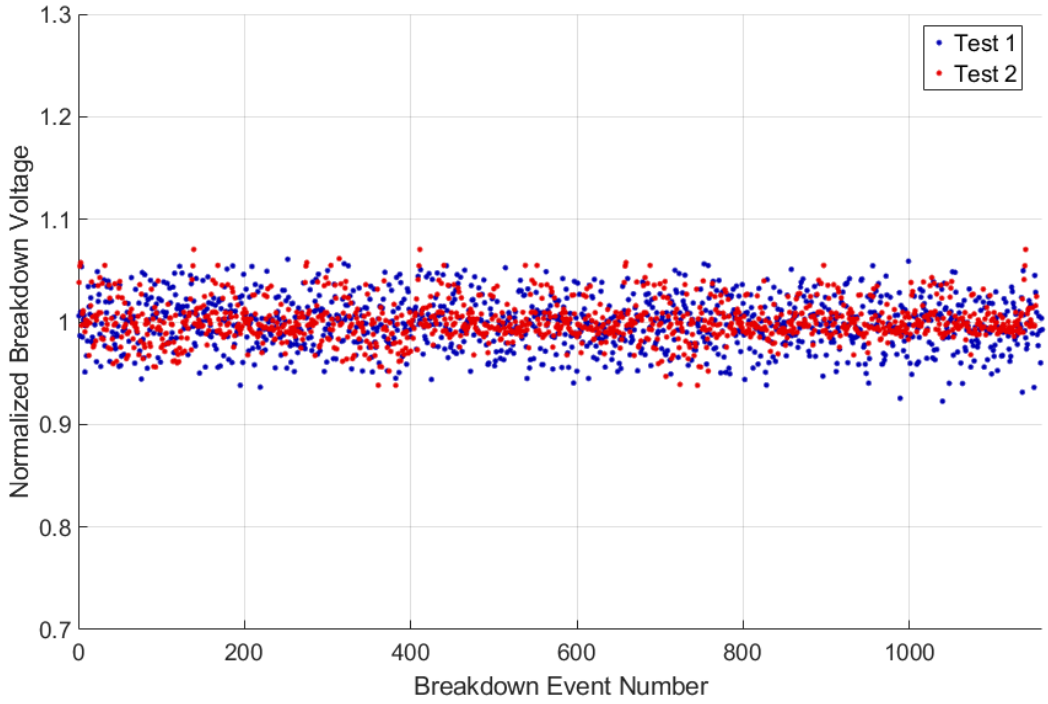

Figure 28: Time-series of normalized N_2 breakdown events.

The results of Figure 28 demonstrate that pure N_2 is also relatively stable over a long period of time. This follows the current understanding that the breakdown of zero-air, which contains oxygen, experiences recombination processes that change the gas chemistry over many closure events. In nitrogen, however, the gas has no other species available for recombination and thus

should cool back into nearly pure N_2. This behavior would not change the overall gas chemistry in the switch volume, meaning that the breakdown voltage should remain constant.

It is important to note that the variance of each dataset is not solely dependent on the gas used. Due to limitations of the charge capacitor at higher voltage operation, the system variance tends to increase at voltage exceeding 45 kV. For SF_6 to have stable pressure operation, the minimum breakdown voltage achievable in the switch system was approximately 50 kV. This higher voltage operation results in the SF_6 data demonstrating higher variance than the other gases, which were operating near 40 kV. The failure criterion, discussed in section 3.7, accounts for such variance and does not quantify failure based on measurement scatter.

3.6 Long Term Measurements of Gas Mixtures

While it is known that SF_6 has stable recombination properties, the mixtures examined in section 3.2 have mostly unknown long-term behavior. The mixture now consists of SF_6, N_2, O_2 and some other trace gases. The breakdown of this mixture has the potential to create many different chemicals which could alter the behavior of the mixture. Thus, it was expected to see the breakdown voltage of the mixture change over time.

Selecting a 50-50 mixture, the same long-term reliability experiment as was performed in 3.5 was run for many thousands of shots. Surprisingly, this data did not demonstrate the reduction of breakdown voltage over time, as was observed in the air dataset. Rather, its voltage remained relatively constant with later shots gaining increased variance. This variance increase was not attributed systematic limitations, as the voltage remained steady at around 40kV. Thus, this increasing variance appears to be an inherent property of the tested mixture rather than an experimental artifact.

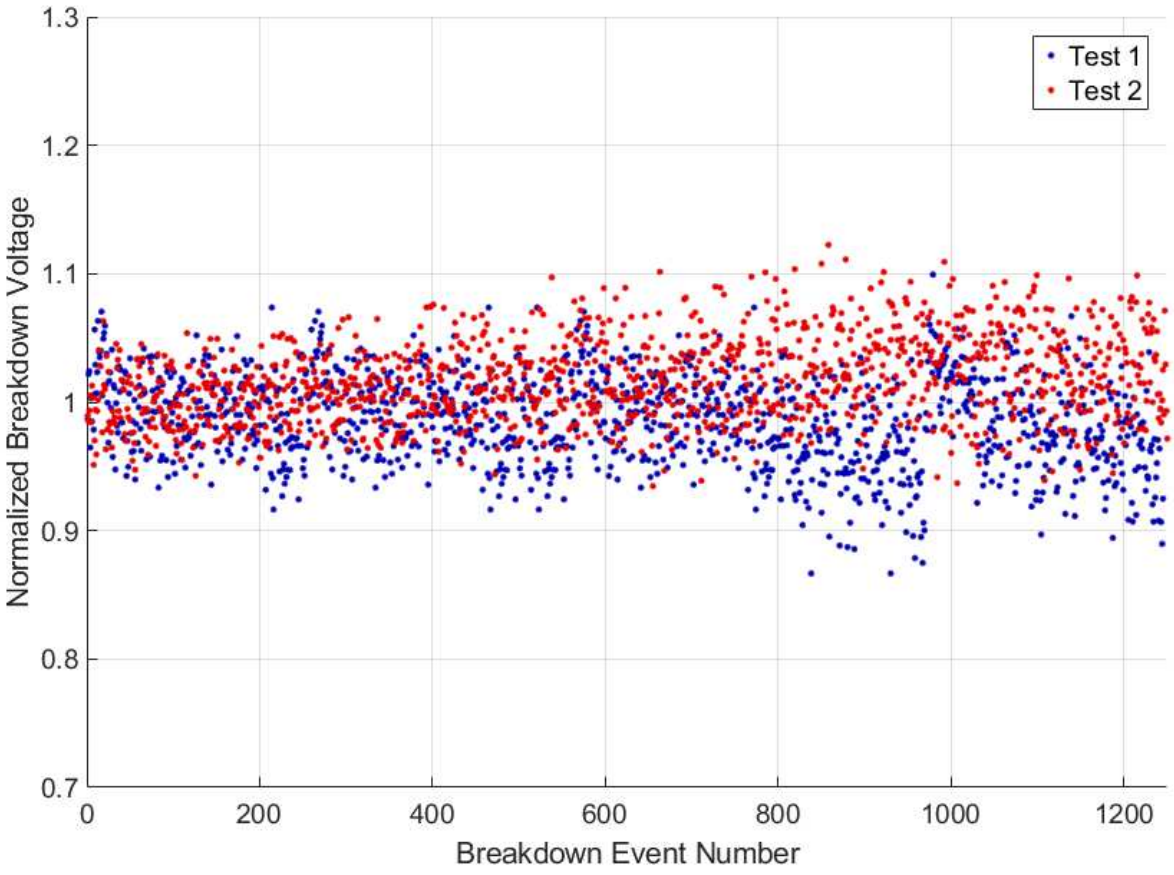

Figure 29: Time-series of normalized 50% zero-air - 50% SF_6 breakdown events.

3.7 Weibull Analysis

To examine the behavior of the tested gas over a long test trial, the data was analyzed to determine the Weibull reliability and hazard rates of all gases or gas mixtures. The reliability represents the overall probability of survival up to a given shot number for a given gas or mixture (Figure 31), while the hazard rate represents the instantaneous probability that a shot will fail at a given shot number (Figure 32). Weibull analysis was selected for this due to its effectiveness in characterizing lifetime and wear-out failures. From a simple examination of the long-term data, especially for air, it is clear that the voltage eventually drifts from its anticipated value, just as a wear-out failure would describe [65], [66].

For this analysis, the failure criterion must be defined. The criterion was chosen to be any breakdown voltage which fell outside of two standard deviations from the baseline mean, where the baseline was determined from the first 100 shots following electrode conditioning. This 100-shot baseline was selected as at this point in the switch operation, no failures have been recorded, as the gas has not yet changed composition enough to impact breakdown voltage. The 2 std failure criterion was selected based on established statistical process control principles and captures approximately 95% of the normal voltage variation, meaning there is only a 5% chance that a stable switch would exceed these limits due to measurement scatter alone [67]. This threshold is commonly used in established literature, and provides good sensitivity to voltage degradation, while preventing excessive false alarms from normal variation. The post-conditioning baseline ensures that this criterion reflects stable switch performance, making the failure definition representative of operational degradation and gas composition changes. The failures for the zero-air data collected during long term testing can be seen in Figure 30.

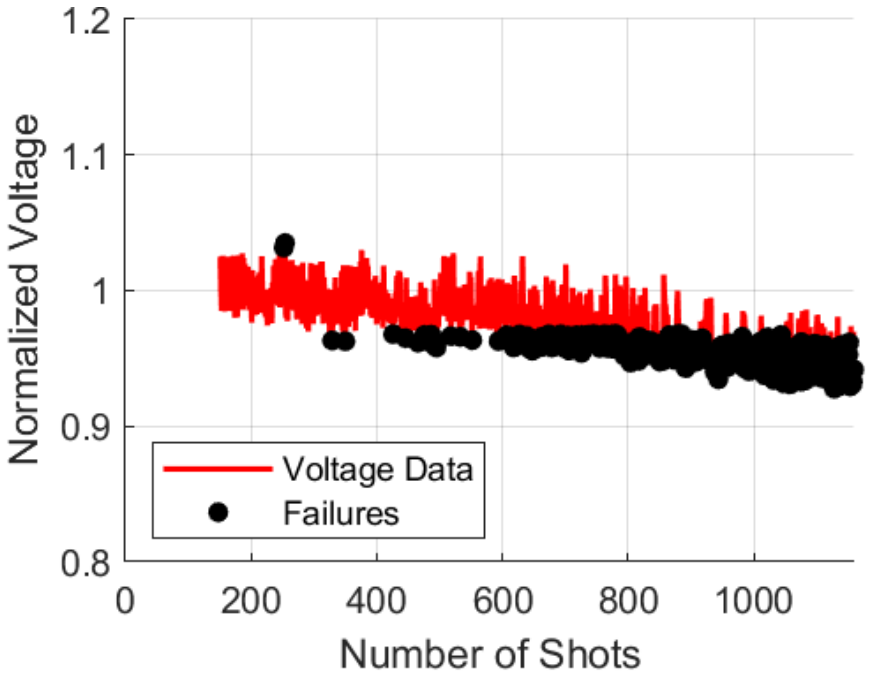

Figure 30: 2 standard deviation failures for long-term zero-air dataset.

This failure condition is specific to the examined system and application and should be adjusted based on the intended operational requirements. Different applications may necessitate more or less stringent failure criteria depending on factors such as acceptable risk levels, operational safety margins, and system criticality. For instance, critical infrastructure or very high voltage applications may require tighter tolerance bands to ensure higher reliability, while research or non-critical applications might accommodate wider tolerance bands to reduce false alarm rates. Additionally, the baseline period may need adjustment based on switch conditioning requirements, gas stabilization time, or the expected operational lifetime of the specific system. The statistical confidence level should also be selected to align with the application's reliability requirements and the consequences of undetected failures versus false alarms.

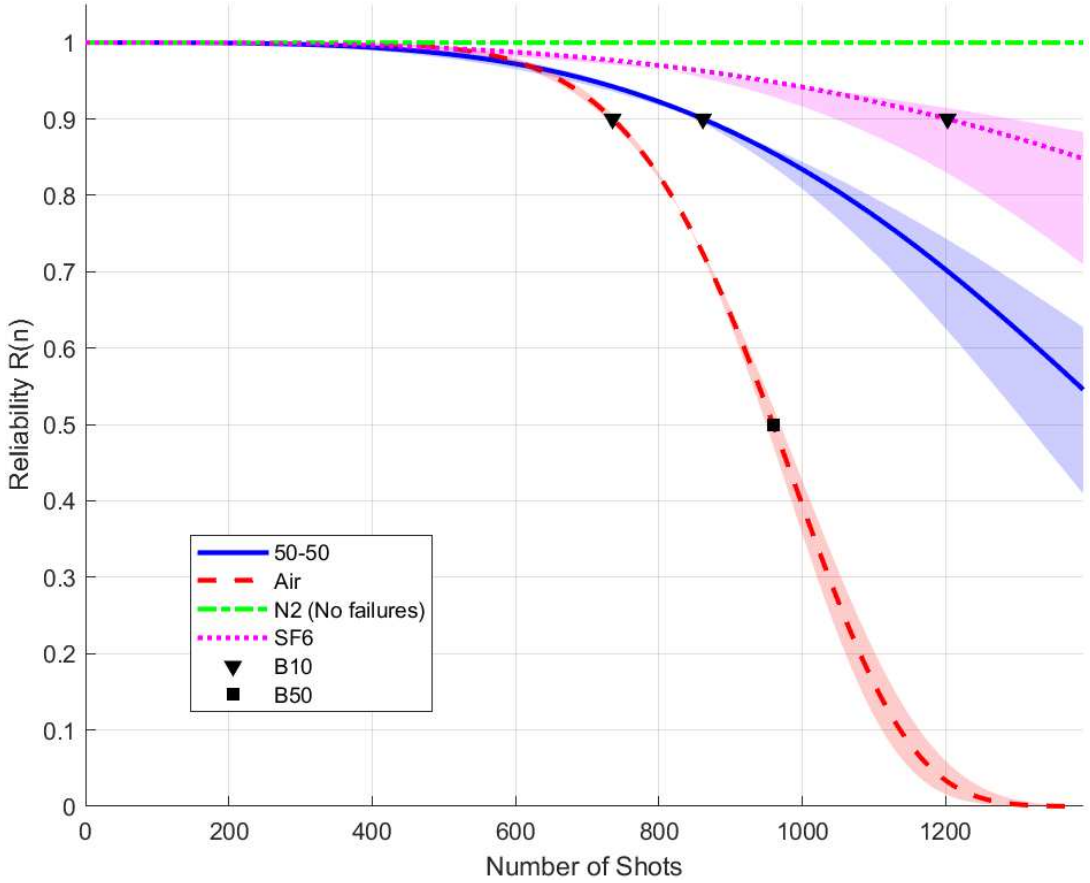

Figure 31: Weibull reliability plots of long-term tests.

The results of this analysis seen in Figure 35 demonstrate that air has the lowest reliability over time, while pure SF_6 and N_2 remain highly reliable over the test run-time. In fact, pure N_2 demonstrated no legitimate failures, indicating that the low reliability stems from the gas composition experiencing chemical changes. The 50% air - 50% SF_6 mixture demonstrated high reliability between that of pure zero-air and pure SF_6. The B10 and B50 markers, representing the shot numbers at which 10% and 50% of the shots have failed are included. The B50 marker is commonly used to predict the end of life for high voltage systems [42]. Pure zero-air reaches this end of life at approximately 950 shots, while the mixture reaches its end of life at approximately 1300, and pure SF_6 fails at approximately 1600 shots. This indicates that such a mixture may be well suited to use in high voltage switch applications.

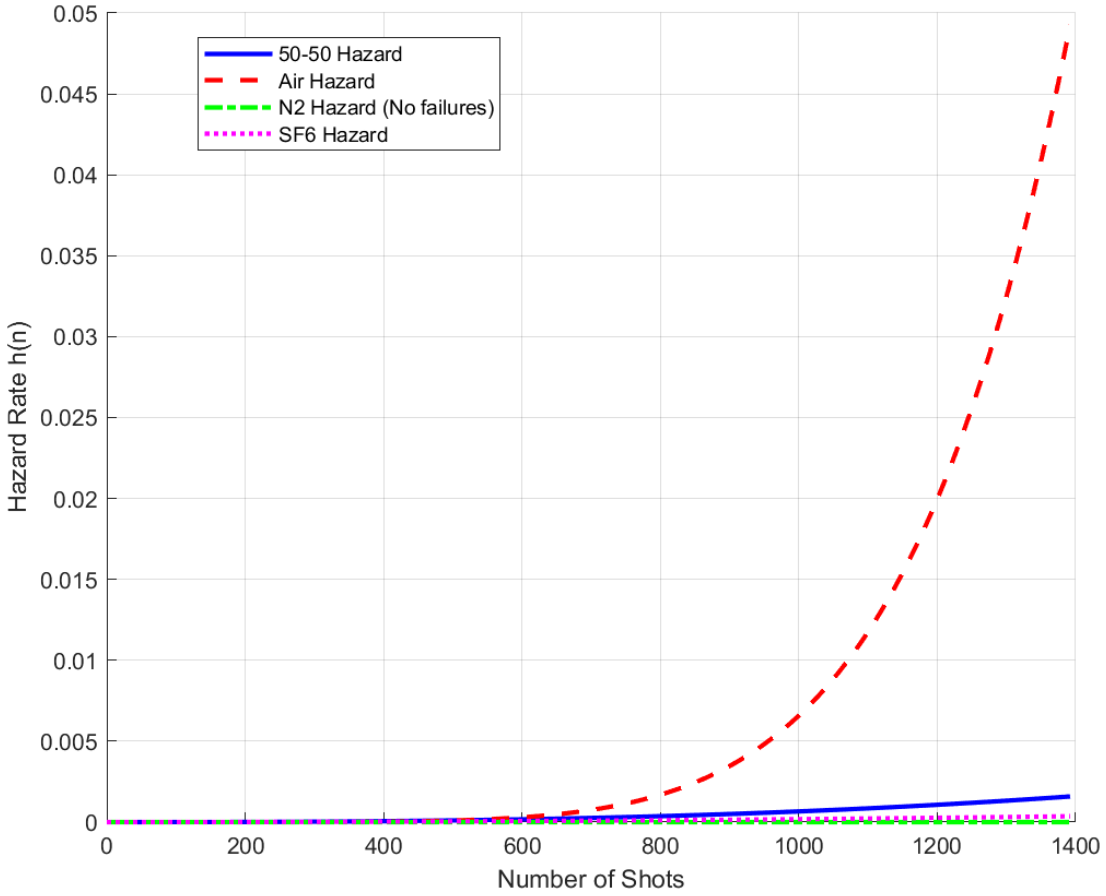

Figure 32: Weibull hazard plots of long-term tests.

4. Conclusions and Future Work

4.1 Conclusion

Through remodeling and conversion of the Pulsed Power and Plasma Science Center (P3SC) at Colorado State University (CSU), this work has created a testing platform designed to evaluate dielectric gases and mixtures for high voltage switch applications in pulsed power and other systems. The enhanced system demonstrates the capability to conduct thousands of breakdown events while maintaining high accuracy and experimental quality. The new, automated approach permits rapid data collection, which is essential as the power industry increasingly seeks alternative gases to sulfur hexafluoride (SF_6).

Paschen curves for pure SF_6, pure zero-air, and three mixtures of zero-air and SF_6 (25%-75%, 50%-50%, and 75%-25%) were created by measuring breakdown voltages and then purging the switch system at several pressure – distance product states. Linear fits were applied to these data, and the linear behavior was validated with statistical analysis. The relative dielectric strength of SF_6 to zero-air was found to be 2.35 to 1, demonstrating good agreement with previously recorded values. These findings support that the behaviors of these mixtures are governed by Paschen's law and fundamental gas physics, independent of experimental variance.

These mixtures exhibit reasonably high hold-off voltages while requiring only minimal amounts of SF_6 addition to the system. Importantly, the mixtures do not require significantly increased operating pressures and could potentially be integrated into current switching systems with minimal design modifications. It was found that for 50 kV operation a 50% zero-air - 50%

SF_6 mixture, could reach equivalent performance to that of pure SF_6 for only a 0.1 MPa operation pressure increase.

The reliability of pure SF_6, pure zero-air, pure N_2, and the 50-50 mixture were examined. This was done by bringing these gases to the proper pressure such that breakdown was achieved at a range of 40-50 kV, the switch was sealed, and the gas was broken down for many thousands of events, allowing the gas to evolve over time. The extensive long-term reliability testing demonstrated that the candidate mixture of 50% zero-air – 50% SF_6 had a reliability similar to that of pure SF_6, far exceeding the performance of pure zero-air. This consistency in long-term operation directly addresses one of the most significant technical barriers to SF_6 replacement in current switching applications.

This research into SF_6 replacement represents an ongoing and important field of study. The P3SC serves as a valuable resource for such research and has the capacity to support the industry's transition to more environmentally sustainable technologies while maintaining the reliability and performance standards essential for critical electrical infrastructure. This experimental work has successfully identified several promising candidate mixtures of zero-air and SF_6 that demonstrate strong potential for implementation in high voltage switchgear.

4.2 Future work

Future work regarding these mixtures presents numerous opportunities for expanding these foundational findings. The automated system enables long-term testing to be readily expanded for longer series analysis, higher voltage operation, or evaluation of additional gas mixtures. Analysis of the gas over extended periods may reveal different reliability characteristics that were not detected in the current work. Additionally, operation at higher voltages may result in the gases or

mixtures evolving in different ways, providing further data supporting these mixtures' use in the power industry. Other gases could be used to create commonly used mixtures with SF_6, such as CO_2 or tetrafluoromethane (CF_4). Other fluorinated compounds are also of interest for the replacement of pure SF_6, and the P3SC has the capacity to quickly examine these gases for their long-term reliability.

System adjustments to achieve higher pressures, voltages, or alternative electrode topologies could be considered to examine gas behavior in different operating regimes. The design of a rotary switch to better isolate electrode surface impacts on testing has already been partially developed. Such a system could be used to investigate alternative gap spacings, electrode material effects, or triggered switching performance. The inclusion of optical access in the design could allow for laser triggering or advanced optical diagnostic techniques.

Thomson scattering measurements have been performed on similar switchgear at CSU for ambient air operation. Investigation of how transient switch performance changes when using these alternative gases may be of interest, especially for high accuracy switchgear used in pulsed power systems. Other optical measurements, such as optical emission spectroscopy, could provide insight into the chemistry of the system during breakdown and whether it evolves over time. Additional electrical measurements using derivative monitors could be employed to examine if the electrical performance changes as the gas evolves or when different gases are used.

Overall, there are many avenues for continued work in this field. The P3SC is in a state where such experimental changes can be quickly implemented with minimal modifications to the overall electrical system. Resistive monitoring and voltage measurements are already available, and the system is fully autonomous, permitting rapid collection of very large datasets. The system

is in a very stable state with minimal losses and high accuracy, so future efforts to improve the system could use the current state of the P3SC as a solid foundation.

BIBLIOGRAPHY

[1] Charles Rose, "Development of a high-voltage laser triggered switch facility including initial optical and electrical diagnostics," M.Sc. Thesis, Colorado State University, Fort Collins, 2019.

[2] I. Smith, "The Early History of Western Pulsed Power," *IEEE Transactions on Plasma Science*, vol. 34, no. 5, pp. 1585–1609, Oct. 2006, doi: 10.1109/TPS.2006.883391.

[3] Anne Van Arsdall, "Pulsed Power at Sandia National Laboratories the first fourty years," 2007.

[4] J. D. Lindl *et al.*, "The physics basis for ignition using indirect-drive targets on the National Ignition Facility," *Phys Plasmas*, vol. 11, no. 2, pp. 339–491, Feb. 2004, doi: 10.1063/1.1578638.

[5] M. E. S. David L. Smith, "ZR Marx capacitor lifetime test results," in *Conference Record of the Twenty-Sixth International Power Modulator Symposium, 2004 and 2004 High-Voltage Workshop.*, IEEE, pp. 530–533. doi: 10.1109/MODSYM.2004.1433631.

[6] Sandia National Laboratory, "Z Pulsed Power Facility ," https://www.sandia.gov/z-machine/.

[7] W. K. Pendleton and A. H. Guenther, "Investigation of a Laser Triggered Spark Gap," *Review of Scientific Instruments*, vol. 36, no. 11, pp. 1546–1550, Nov. 1965, doi: 10.1063/1.1719388.

[8] W. R. Cravey et al., "Picosecond High Pressure Gas Switch Experiment," Livermore, Jun. 1993.

[9] J. Gottfried, C. E. Rose, and A. P. Yalin, "Optical and Electrical Diagnostics of a High-Voltage Laser-Triggered Switch with Variable Impedance Load," in *AIAA SCITECH 2023 Forum*, Reston, Virginia: American Institute of Aeronautics and Astronautics, Jan. 2023. doi: 10.2514/6.2023-2384.

[10] J. A. Gottfried, C. E. Rose, S. Simpson, and A. P. Yalin, "Collective Thomson scattering measurement of plasma evolution during the current pulse in a laser-triggered switch," *Appl Phys Lett*, vol. 121, no. 24, Dec. 2022, doi: 10.1063/5.0131471.

[11] J. M. Meek, “A Theory of Spark Discharge,” *Physical Review*, vol. 57, no. 8, pp. 722–728, Apr. 1940, doi: 10.1103/PhysRev.57.722.

[12] Y. Raizer, *Gas Discharge Physis*, 1st ed. Moscow: Springer Berlin, Heidelberg, 1991.

[13] S. Zheng, Z. Kang, L. Li, A. Zhang, K. Zhao, and Y. Zhou, “Influence of series RC circuit parameters on the streamer discharge process of gas spark switch,” *Vacuum*, vol. 193, p. 110518, 2021, doi: https://doi.org/10.1016/j.vacuum.2021.110518.

[14] L. P. Bradley, “Highly overvolted gas spark gaps for electron beam generators,” in *Proceedings of the 1971 Particle Accelerator Conference*, Chicago, IL, Mar. 1971, pp. 477–480.

[15] D. J. Bradley, J. F. Higgins, M. H. Key, and S. Majumdar, “A simple laser-triggered spark gap for kilovolt pulses of accurately variable timing,” *Opto-electronics*, vol. 1, no. 1, pp. 62–64, Feb. 1969, doi: 10.1007/BF01476795.

[16] S. Simpson *et al.*, “Triggering of a High Pressure Air-filled High Voltage Spark Gap Switch Using Fiber Delivered Laser Induced Plasmas Resulting in Sub-nanosecond Jitter at Low Percentages of Self-Break,” in *IEEE Pulsed Power Conference*, Brighton, United Kingdom, Jun. 2017.

[17] F. Paschen, “Ueber die zum Funkenübergang in Luft, Wasserstoff und Kohlensäure bei verschiedenen Drucken erforderliche Potentialdifferenz,” *Ann Phys*, vol. 273, no. 5, pp. 69–96, Jan. 1889, doi: 10.1002/andp.18892730505.

[18] Sessler G. M. and Kristiansen J. E., “Breakdown of air in uniform and nonuniform fields,” *J Appl Phys*, vol. 38, no. 11, pp. 4576–4580, Oct. 1967.

[19] Martin T. H., Seamen J. F., and Jobe D. O., “Energy Losses in Switches,” in *Ninth IEEE International Pulsed Power Conference*, 1993, pp. 463–470.

[20] J. S. Townsend, *Electricity in Gases*. Oxford, U.K.: Clarendon Pres, 1915.

[21] L. M. Chanin and G. D. Rork, “Experimental Determinations of the First Townsend Ionization Coefficient in Helium,” *Physical Review*, vol. 133, no. 4A, pp. 1005-A1009, Feb. 1964, doi: 10.1103/PhysRev.133.1005.

[22] E. Kuffel and W. S. Zaengl, *High Voltage Engineering: Fundamentals*, 2nd ed. Butterworth-Heinemann, 2000.

[23] K. T. A. L. Burm, “Calculation of the Townsend Discharge Coefficients and the Paschen Curve Coefficients,” *Contributions to Plasma Physics*, vol. 47, no. 3, pp. 177–182, May 2007, doi: 10.1002/ctpp.200710025.

[24] Martin T. H., “Pulse Charged Gas Breakdown,” in *Fifth IEEE Pulsed Power Conference*, 1985, pp. 74–83.

[25] Braginskii S. I., “Transport Processes in a Plasma,” *Reviews of Plasma Physics*, vol. 1, pp. 205–311, Oct. 1965.

[26] Chen F. F., *Introduction to Plasma Physics and Controlled Fusion*, 3rd ed., vol. 1. Switzerland: Springer, 2016.

[27] V. V Apollonov, A. A. Belevtsev, S. Y. Kazantsev, A. V Saifulin, and K. N. Firsov, “Ion — ion recombination in SF6 and in SF6 — C2H6 mixtures for high values of E/N,” *Quantum Elec (Woodbury)*, vol. 31, no. 7, pp. 629–633, Jul. 2001, doi: 10.1070/QE2001v031n07ABEH002017.

[28] S. Díaz, J. Nuez, K. Berdugo, and K. Gomez, “Study of technologies implemented in the operation of SF6 switches,” in *IOP Conference Series: Materials Science and Engineering*, Institute of Physics Publishing, Jun. 2020. doi: 10.1088/1757-899X/872/1/012041.

[29] N. Malik and A. Qureshi, “A Review of Electrical Breakdown in Mixtures of SF6 and Other Gases,” *IEEE Transactions on Electrical Insulation*, vol. EI-14, no. 1, pp. 1–13, Feb. 1979, doi: 10.1109/TEI.1979.298198.

[30] A. Lee and L. S. Frost, “Interruption Capability of Gases and Gas Mixtures in a Puffer-Type Interrupter,” *IEEE Transactions on Plasma Science*, vol. 8, no. 4, pp. 362–367, 1980, doi: 10.1109/TPS.1980.4317341.

[31] R. Yang *et al.*, “Decomposition Characteristics of SF6 under Arc Discharge and the Effects of Trace H2O, O2, and PTFE Vapour on Its By-Products,” *Energies (Basel)*, vol. 14, no. 2, 2021, doi: 10.3390/en14020414.

[32] Nicola Garaboldi and Javier Mantilla, “Electrical Wear in High-Voltage Circuit Breakers Using SF6 Alternative Gases ,” *International Electrical Testing Association* , no. Industry Topics, May 2021.

[33] Y. Kieffel, F. Biquez, P. Ponchon, and Alstom, “SF6 alternative development for high voltage switchgears,” 2015. doi: 10.1109/ICACACT.2014.7223577.

[34] A. Beroual and A. (Manu) Haddad, “Recent Advances in the Quest for a New Insulation Gas with a Low Impact on the Environment to Replace Sulfur Hexafluoride (SF6) Gas in High-Voltage Power Network Applications,” *Energies (Basel)*, vol. 10, no. 8, p. 1216, Aug. 2017, doi: 10.3390/en10081216.

[35] X. Li, H. Zhao, and A. Murphy, “SF6-alternative gases for application in gas-insulated switchgear,” *J Phys D Appl Phys*, vol. 51, Apr. 2018, doi: 10.1088/1361-6463/aab314.

[36] A. Romero, L. Racz, A. Matrai, T. Bokor, and R. Cselko, “A review of sulfur-hexafluoride reduction by dielectric coatings and alternative gases,” in *2017 6th International Youth*

Conference on Energy (IYCE), IEEE, Jun. 2017, pp. 1–5. doi: 10.1109/IYCE.2017.8003750.

[37] S. Miller, R. D. Curry, O. Johns, M. Rawson, and R. B. Spielman, "High Pressure Operation of Ultra-Zero Air as a Replacement for SF6," in *2023 IEEE Pulsed Power Conference (PPC)*, IEEE, Jun. 2023, pp. 1–3. doi: 10.1109/PPC47928.2023.10310674.

[38] Y. Kieffel and F. Biquez, "SF6 alternative development for high voltage switchgears," Apr. 2015, pp. 379–383. doi: 10.1109/ICACACT.2014.7223577.

[39] W. M. Leeds, T. E. Browne, and A. P. Strom, "The use of SF6 for high-power arc quenching," *Electrical Engineering*, vol. 76, no. 9, pp. 788–791, Sep. 1957, doi: 10.1109/EE.1957.6442711.

[40] X. Li, H. Zhao, and A. B. Murphy, "SF6 - alternative gases for application in gas-insulated switchgear," *J Phys D Appl Phys*, vol. 51, no. 15, p. 153001, Apr. 2018, doi: 10.1088/1361-6463/aab314.

[41] A. L. Donaldson, T. G. Engel, and Kristiansen M., "State-of-the-art insulator and electrode materials for use in high current high energy switching," *Transactions on Magnetics*, vol. 25, no. 1, Jan. 1989.

[42] IEEE Standard, "IEEE Standard Test Procedures for AC High-Voltage Circuit Breakers with Rated Maximum Voltage Above 1000V - IEEE Std. C37.09-2018," 2018, *IEEE*.

[43] W. A. Stygar, R. B. Spielman, and H. C. et. al Ives, "D-Dot and B-Dot Monitors for Z-Vacuum-Section Power-Flow Measurements," Albuquerque, New Mexico, USA, 1997.

[44] I. A. Metwally, "Self-Integrating Rogowski Coil for High-Impulse Current Measurement," *IEEE Trans Instrum Meas*, vol. 59, no. 2, pp. 353–360, Feb. 2010, doi: 10.1109/TIM.2009.2023821.

[45] M. Alonso and J. Gruenwald, "Diagnostics and stabilisation of fusion relevant, laser-accelerated high-energetic proton beams with miniaturised Rogowski coils. 3rd European Conference on Plasma Diagnostics (ECPD), 6-9 May 2019, Lisbon, Portugal," May 2019.

[46] Ahmad Al Agry, "Calibration of Electromagnetic Dot Sensor - Part 1: B-Dot Mode," *IEEE Sens J*, vol. 14, no. 9, Sep. 2014.

[47] I. A. et. al Metwally, "Coaxial D-Dot Probe: Design and Testing," Mansoura, Egypt.

[48] Ibrahim A. Metwally, "D-Dot Probe for Fast-Front High-Voltage Measurement," *IEEE Trans Instrum Meas*, vol. 59, no. No. 8, Aug. 2010.

[49] Ahmad Al Agry, "Calibration of Electromagnetic Dot Sensor - Part 2: D-Dot Mode," *IEEE Sensors Journal* , vol. 14, no. No. 9, Sep. 2014.

[50] A. I. Gerasimov, “Aqueous-solution high-voltage resistors: Development, study, and application (review),” *Instruments and Experimental Techniques*, vol. 49, no. 1, pp. 1–26, Jan. 2006, doi: 10.1134/S0020441206010015.

[51] Y. Fu, J. Krek, P. Zhang, and J. P. Verboncoeur, “Gas Breakdown in Microgaps With a Surface Protrusion On the Electrode,” *IEEE Transactions on Plasma Science*, vol. 47, no. 5, pp. 2011–2019, May 2019, doi: 10.1109/TPS.2018.2878011.

[52] G. Meng, Y. Cheng, X. Gao, K. Wang, C. Dong, and B. Zhu, “In-situ optical observation of dynamic breakdown process across microgaps at atmospheric pressure,” *IEEE Transactions on Dielectrics and Electrical Insulation*, vol. 25, no. 4, pp. 1502–1507, Aug. 2018, doi: 10.1109/TDEI.2018.007017.

[53] A. M. Loveless and A. L. Garner, “A universal theory for gas breakdown from microscale to the classical Paschen law,” *Phys Plasmas*, vol. 24, no. 11, Nov. 2017, doi: 10.1063/1.5004654.

[54] I. W. McAllister, “Illusory Paschen curves associated with strongly electronegative gases,” *IEEE Transactions on Electrical Insulation*, vol. 26, no. 3, pp. 391–397, Jun. 1991, doi: 10.1109/14.85109.

[55] Y. D. Korolev and N. M. Bykov, “High-Voltage Spark Gap in a Regime of Subnanosecond Switching,” *IEEE Transactions on Plasma Science*, vol. 40, no. 10, pp. 2443–2448, Oct. 2012, doi: 10.1109/TPS.2011.2178041.

[56] W. J. Carey, A. J. Wiebe, R. D. Nord, and L. L. Altgilbers, “Characterization of Paschen curve anomolies at high P*D values,” in *2011 IEEE Pulsed Power Conference*, IEEE, Jun. 2011, pp. 741–744. doi: 10.1109/PPC.2011.6191503.

[57] E. Husain and R. S. Nema, “Analysis of Paschen Curves for air, N2 and SF6 Using the Townsend Breakdown Equation,” *IEEE Transactions on Electrical Insulation*, vol. EI-17, no. 4, pp. 350–353, Aug. 1982, doi: 10.1109/TEI.1982.298506.

[58] Y. Fu, J. Krek, P. Zhang, and J. P. Verboncoeur, “Evaluating microgap breakdown mode transition with electric field non-uniformity,” *Plasma Sources Sci Technol*, vol. 27, no. 9, p. 095014, Sep. 2018, doi: 10.1088/1361-6595/aadf56.

[59] I. W. McAllister and G. C. Crichton, “The concept of Paschen’s law with reference to SF6,” *J Phys D Appl Phys*, vol. 20, no. 11, pp. 1537–1539, Nov. 1987, doi: 10.1088/0022-3727/20/11/027.

[60] T. Ishii *et al.*, “Insulating Characteristics of Small SF6 Gas Gaps under Lightning Impulse Voltages,” in *Gaseous Dielectrics VI*, Boston, MA: Springer US, 1991, pp. 261–266. doi: 10.1007/978-1-4615-3706-9_32.

[61] S. S. Shapiro and M. B. Wilk, “An Analysis of Variance Test for Normality (Complete Samples),” *Biometrika*, vol. 52, no. 3/4, p. 591, Dec. 1965, doi: 10.2307/2333709.

[62] J. R. Taylor, *An Introduction to Error Analysis: The Study of Uncertainties in Physical Measurements*, 2nd ed. University Science Books, ISBN: 978-0-935702-75-0, 1997.

[63] K. Mardikyan, “Breakdown strength of air, SF6 and a mixture of air plus SF6 containing a small amount of SF6,” *European Transactions on Electrical Power*, vol. 9, no. 5, pp. 313–316, Sep. 1999, doi: 10.1002/etep.4450090506.

[64] A. Hopf, J. A. Britton, M. Rossner, and F. Berger, “Dielectric strength of SF6 substitutes, alternative insulation gases and PFC-gas-mixtures,” in *2017 IEEE Electrical Insulation Conference (EIC)*, IEEE, Jun. 2017, pp. 209–212. doi: 10.1109/EIC.2017.8004635.

[65] G. U. Crevecoeur, “A model for the integrity assessment of ageing repairable systems,” *IEEE Trans Reliab*, vol. 42, no. 1, pp. 148–155, Mar. 1993, doi: 10.1109/24.210287.

[66] Weibull W., “A Statistical Distribution Function of Wide Applicability,” *Journal of Applied Mechancis*, vol. vol.18, no. 3, Aug. 1951.

[67] D. C. Montgomery, *Introduction to Statistical Quality Control*, 8th ed. John Wiley & Sons, 2019.